

Physical and kinematical characteristics of Wolf-Rayet central stars and their host planetary nebulae

Awad, Z and Ali, A.

Department of Astronomy, Space Science and Meteorology, Faculty of Science, Cairo University,
 12613 Giza, Egypt;
zma@sci.cu.edu.eg, afouad@sci.cu.edu.eg

Received 2022 month day; accepted 2023 May 24

Abstract We addressed the physical and kinematical properties of Wolf – Rayet [WR] central stars (CSs) and their hosting planetary nebulae (PNe). The studied sample comprises all [WR] CSs that are currently known. The analysis is based on recent observations of the parallax, proper motion, and color index of [WR] CSs from the Gaia space mission's early third release (eDR3) catalog, as well as common nebular characteristics. The results revealed an evolutionary sequence, in terms of decreasing T_{eff} , from the early hot [WO 1] to the late cold [WC 12] stars. This evolutionary sequence extends beyond [WR] CS temperature and luminosity to additional CS and nebular characteristics. The statistical analysis showed that the mean final stellar mass and evolutionary age of the [WR] CS sample are $0.595 \pm 0.13 M_{\odot}$ and 9449 ± 2437 yr, respectively, with a mean nebular dynamical age of 7270 ± 1380 yr. In addition, we recognized that the color of the majority ($\sim 85\%$) of [WR] CSs tends to be red rather than their genuine blue color. The analysis showed that two-thirds of the apparent red color of most [WR]s is attributed to the interstellar extinction whereas the other one-third is due to the PN self-extinction effect.

Key words: Planetary nebulae: general – Methods: kinematics - Stars: Wolf – Rayet [WR]

1 INTRODUCTION

Understanding the late stages of stellar evolution provides us with insight into the evolution of our Galaxy since these phases enrich the interstellar medium (ISM) with a lot of elements created inside these stars via nuclear fusion (Williams 2003). It is now well-established that the evolution of low- and intermediate- mass stars ($0.8 < M (M_{\odot}) < 8$) passes through a transition stage known as planetary nebula (PN). This stage is halfway between the post asymptotic giant branch (post-AGB), in which stars have hydrogen (H) and helium (He) burning shells, and the white dwarf (WD), in which stars have carbon (C) -oxygen (O) cores (Werner & Herwig 2006). Central stars (CS)s of PNe (PNCSs) are often not easy to detect because they are: (1) optically faint ($\sim 60\%$ have $V > 15.5$ mag), (2) masked by the nebular emission, and sometimes are (3) shifted from the PN center. Based on the H abundance in the atmosphere of CSs, as derived from their spectral analysis, astronomers showed that CSs can fall into two categories: H-rich and H-deficient (Mendez 1991). H-deficient CSs show higher abundances of He and C with a small amount of H (or almost H free) compared to their H-rich peers. Stellar spectra of H-deficient CSs are dominated by broad and intense emission lines typical of Wolf-Rayet (WR) massive stars. In order to distinguish WR CSs from the well-known massive WRs, van der Hucht et al. (1981)

introduced the [WR] notation to denote WR CSs. [WR]s have two main sub-types: carbon-rich [WC], that is dominated by C III 5696Å lines, and oxygen-rich [WO], that is dominated by highly ionized lines of C and O such as C IV 5806Å and O VI 3822Å line (e.g. [Weidmann & Gamen 2011](#), and references therein).

Early classification of massive WR was qualitative and hence subjective to observers (e.g. [Beals 1938](#); [Hiltner & Schild 1966](#)). The classical WRs were grouped into nitrogen (N) and C stars (WN and WC; respectively) based on the dominant emission features detected in their spectra. According to the ratio between the spectral lines of WN and WC stars, [Beals \(1938\)](#) divided them into sub-types designed as WN 5 to WN 8 and WC 6 to WC 8. This classification was then improved by including the line width of the observed emission lines ([Hiltner & Schild 1966](#)).

[Smith et al. \(1990\)](#) reported a new quantitative scheme to define the sub-types WC 4 to WC 9. In this scheme, the principle identifier for WC 4 - 6 stars is the line ratio C III λ 5696 / O V λ 5590, while for WC 7 - 9 stars is the line ratio C IV λ 5808 / C III λ 5696. [Smith et al. \(1994\)](#) suggested a new method to define the WN 9 - 11 sub-types, while [Smith et al. \(1996\)](#) used the H abundance and the He II λ 5411 / He I λ 5875 line ratio to discriminate the ionization subclass of WN 2 - 9.

[Barlow & Hummer \(1982\)](#) proposed that the WO sequence is an evolutionary stage after the WCs and designated the WO sub-types according to the degree of O ionisation to be WO 1 to WO 4; from the greatest to the weakest ionized O lines. [Kingsburgh et al. \(1995\)](#) defined quantitative spectral type criteria for the whole WO class, and extended the sub-types to include the subclass WO 5 which has an equivalent width of O VI λ 3811,43 / O V λ 5590 line ~ 1 compared to 4 in the WO 4 subclass. Moreover, the authors used the C III λ 5696 emission line to distinguish WOs from WC 4. The classification of WO and WC stars was then revisited by [Crowther et al. \(1998\)](#) using high-quality optical observations of twenty WR stars.

[Acker & Neiner \(2003\)](#) have constructed a grid of line intensities normalized to the C IV 5806Å line and found that their new classification of the hot ([WO 1-4]) and cool ([WC 4-11]) CSs is consistent with that of [Crowther et al. \(1998\)](#). This classification is based on the evolution of both the effective temperature (T_{eff}) and stellar winds, where the [WR] evolutionary sequence, in terms of decreasing T_{eff} , can be summarized as [WO 1]-[WO 4] \rightarrow [WC 4]-[WC 11].

The existence of He, C, and O absorption lines in the spectra of some H-deficient stars led to the definition of a new class known as PG 1159, named after the discovery of its prototype star PG 1159–035 (e.g. [Napiwotzki & Schoenberner 1991](#); and references therein).

Furthermore, there is a class of CSs with spectra similar to those of [WR] stars but with weaker intensities, narrower line widths, and not required to be of H-poor atmospheres. This class is the so-called weak emission line stars (*WELs*; e.g. [Tylenda et al. 1993](#) and [DePew et al. 2011](#)). The high resolution and integral field unit (IFU) spectra of numerous PNe hosting *WEL* central stars cast doubt on the classification of *WELs* ([Weidmann et al. 2015](#)). The majority of the characteristic spectral lines of *WELs* had been reported to be of nebular origin rather than of CS origin (e.g. [Basurah et al. 2016](#); [Ali et al. 2016](#); [Ali & Dopita 2019](#)). Moreover, the results of [Miszalski et al. \(2011\)](#) indicated that the classification of *WELs* is likely to be attributable to irradiation of the secondary companion in a close binary system.

[Girard et al. \(2007\)](#) studied the chemical compositions and other aspects of PNe surrounding *WELs*, [WC] and [WO] CSs. The results revealed no substantial variations in the electron temperatures, elemental abundances and the amount of ionizing photons among these types of PNe and the normal PNe. However, they show some differences in their IR properties in which CSs of *WELs* class appeared bluer than the other [WR] CSs. In addition, the data analysis supported the hypothesis which proposes an evolutionary sequence from cool [WC 11] inside dense, low-excitation nebulae to hot [WO 1] inside low-density, high-excitation nebulae. Also, the results showed no correlation between the PN properties (e.g. the number of ionizing photons, nebular excitation, and electron temperature and density) for PNe associated with *WELs* and the other [WR]PNe. This result indicates that *WELs* PNe may account for a separate class of objects with a variety of nebular properties that may arise due to confounding effects.

[Peña et al. \(2013\)](#) examined the circular (V_{cir}) and radial peculiar (V_{pec}) velocities in samples of *WELs* and [WR] CSs, where they found that [WR]s are concentrated in the Galactic thin-disk more than

WELs and normal PNe indicating a younger population. Furthermore, the vast majority of [WR] nebulae are of Pimbert's type II ($V_{\text{pec}} \sim 60 \text{ km/s}$), with a small percentage of type III ($V_{\text{pec}} > 60 \text{ km/s}$). These results show that the [WR] phenomena can occur in objects of any stellar mass and age.

Recently, [Muthumariappan & Parthasarathy \(2020\)](#) used infrared (IR) photometric data to derive the IR properties of three samples of PNe associated with [WR], *WELs*, and normal CSs. The results revealed a tight correlation of decreasing the dust temperature (T_d) with the nebular age: ([WCE]: [WO1] to [WC4]) → ([WCg]: [WC5] to [WC8]) → ([WCL]: [WC 9] to [WC 11]); where [WCE], [WCg], and [WCL] are the early, intermediate, and late types of [WR], respectively. Additionally, the IR luminosity (L_{IR}) of PN show a strong anti-correlation with the PN age and dust mass (m_d), while the dust-to-gas mass ratio (m_d/m_g) does not change noticeably with the PN evolution. More recent studies reported that early types [WR] ([WCE]: [WO1]-[WC5]) have high T_{eff} , ranging from 80,000 K to 150,000 K, while the late types ([WCL]:[WC6]-[WC11]) have T_{eff} between 20,000 K and 80,000 K ([Danehkar 2021](#); and references therein).

[Peimbert \(1978\)](#), introduced a chemical classification for PNe, based on the elemental abundances of He, O, and N relative to H. This classification was revised by [Quireza et al. \(2007\)](#), where they combined the chemical properties of the PN with some kinematical parameters of the CS such as the Galactic height (Z), V_{pec} , and the initial mass. The results showed that PNe of types I, IIa, and IIb are of population I (pop I) that occupy the Galactic thin-disk while PNe of type III populate the Galactic thick-disk and are of population II (pop II).

Motivated by the huge improvements in the observations of the stellar photometry, distance and proper motion occur in the early third data release (*hereafter eDR3*) of the Gaia mission¹ ([Gaia Collaboration 2020](#)), we performed a computational and statistical analysis on a sample of PNe associated with [WR] to derive the main characteristics of both the CS and their hosting nebulae.

This paper is organized as follows: Section 2 describes the strategy of selecting and filtering our data sample. The main properties of [WR] CSs and their hosting nebulae are presented in Section 3 and 4, respectively, while the origin of [WR] CSs is discussed in Section 5. Finally, we summarize the present work and drew some key conclusions in Section 6.

2 THE DATA SAMPLE

The eDR3, which includes the astrometric and photometric data for ~ 1.8 billion sources, showed several improvements over the previous second release (DR2; [Gaia Collaboration et al. 2018](#)). The astrometric parameters include the Galactic positions (l, b), proper motion components (μ_α, μ_δ) and the parallax (ϖ) while the photometric data includes stellar magnitudes in the visual (G), blue (G_{BP}) and red (G_{RP}) filters for sources as faint as 21 magnitude. The accuracy of the astrometric parameters in eDR3 has been enhanced by a factor of 2 in the proper motion and of ~ 1.5 in the parallax whereas astrometric errors were reduced by 30 - 40% for the parallax and by a factor of 2.5 for the proper motion.

In this work, we extracted a sample of PNe associated with [WR] nuclei from the PN CSs catalog of [Weidmann et al. \(2020\)](#) which is electronically available, openly, in the Vizier database². After collecting the [WR]s sample from the catalogue, we performed a cross-matching between the coordinates of the selected objects and their corresponding values given in both the HASH catalogue³ and the SIMBAD database⁴. Moreover, we checked the CS position using Aladin Sky Atlas⁵ because a few number of CSs are shifted from their geometric centres in PNe as a result of the interaction with the ISM. Recently, [Chornay & Walton \(2020\)](#) used an automated method to identify the positions of central stars using the Gaia DR2 database. We compared our sample to their catalog and found that only 15 of our sources (out of 120; 12.5%) are not included in their list. This finding supports the accuracy of the method we adopted in identifying our Gaia eDR3 sources.

¹ Details on Gaia mission: <http://sci.esa.int/gaia/>

² link to [Weidmann et al. \(2020\)](#) catalog: <https://cdsarc.cds.unistra.fr/viz-bin/cat/J/A+A/640/A10>

³ HASH: <http://planetarynebulae.net/EN/hash.php>

⁴ SIMBAD: <https://simbad.u-strasbg.fr/simbad/simbad/simbad/simbad/simbad/simbad/>

⁵ Aladin: <https://aladin.u-strasbg.fr/>

Weidmann et al. (2020) catalog contains data for ~ 620 CSs, collected from numerous literature surveys, including the CS spectral classification as well as the values of surface gravity (g), effective temperature and luminosity (L) for 56.3%, 69.8%, 60.5% of the total number of sources; respectively. The visual magnitude of $\sim 74.4\%$ of the sources is also provided. In this work, the CS luminosity which is listed in Weidmann et al. (2020) was updated using the derived distance from the recent Gaia eDR3 parallax. Angular radii, of the entire PN sample, as well as distances for the objects of unknown, negative, and/or highly uncertain parallaxes ($\sigma_{\varpi} \geq 50\%$) are obtained from Frew et al. (2016) while radial velocities are collected from Durand et al. (1998) unless stated otherwise. The expansion velocities were collected from Acker et al. (1992) except for PNe of unknown measurement, we used the standard value of 20 km/s (Weinberger 1989).

A summary of the selected sample, which includes 120 [WR]s classified into: 79 [WC], 38 [WO] and 3 [WN], is given in Table 1. The table lists the PN name, [WR] classification, Gaia eDR3 designation, Galactic (l, b) and Equatorial (α, δ) coordinates in degrees. In addition, the proper motion in mas/yr, parallax in mas, distance (D) in pc, PN angular radius (θ) in arcsec, radial velocity (V_r) in km/s and nebular expansion velocity (V_{exp}) in km/s and their uncertainties are given in Table 2. It is worth noting that the unique serial number given for each object, in Tables 1 and 2, has been kept fixed throughout this study. The serial ranges 1-79, 80-117 and 118-120 refer to [WC], [WO] and [WN] sub-classes, respectively.

To make the results of the current study more precise and informative, we omitted the three [WN] sources from the analysis and focused on the [WO] and [WC] sources due to their large number and their indicated evolutionary sequence (Acker & Neiner 2003). Therefore, the number of sources in our sample is 117. We divided the data sample into two [WR] groups: early group [WRE] (includes [WO 1] - [WC5]) and late group [WRL] (includes [WC 6] - [WC 12]), following Danehkar (2021). We omitted objects of uncertain and multiple classifications; e.g. objects of class [WC 5/6]. The number of excluded objects is 12, which represents 10% of the entire [WR] sample.

Table 1: The basic properties of a sample of the entire [WR] studied sample. The complete table is given in Table A.1 in the Appendix.

serial	PN Name	[WR] type	Gaia eDR3 Source ID	Galactic Coordinates		Equatorial Coordinates	
				$l(^{\circ})$	$b(^{\circ})$	R.A($^{\circ}$)	Dec.($^{\circ}$)
1	PN H 1-62	[WC 10-11]	4045771305065496832	0.0100	- 6.8504	273.3248	- 32.3286
2	PN M 2-20	[WC 5-6]	4056503259966429440	0.4132	- 1.9893	268.6055	- 29.6023
3	PN H 1-47	[WC 11]?	4062301564840251520	1.2949	- 3.0402	270.1568	- 29.3640

Table 2: An example of the proper motion ($\mu_{\alpha}, \mu_{\delta}$), parallax (ϖ), and distance (D) as well as the nebular angular radius (θ), radial velocity (V_r) and expansion velocity (V_{exp}) for a sample of the studied entire sample. Distances marked with the \dagger symbol are taken from Frew et al. (2016). Full data are listed in Table A.2 in the Appendix.

Serial	$\mu_{\alpha} \pm e$ (mas/yr)	$\mu_{\delta} \pm e$ (mas/yr)	$\varpi \pm e$ (mas)	$D \pm e$ pc	θ (arcmin)	$V_r \pm e$ (km/s)	V_{exp} (km/s)
1	-3.681 ± 0.040	-3.597 ± 0.030	0.047 ± 0.034	6970 ± 2430	2.25	-86.6 ± 4.7	20
2	2.778 ± 0.268	-10.904 ± 0.172	-1.930 ± 0.240	$\dagger 7613 \pm 1670$	1.88	58.7 ± 15.0	20
3	1.323 ± 0.063	-7.017 ± 0.044	0.091 ± 0.050	9757 ± 2139	1.25	107.5 ± 3.1	20

3 CHARACTERIZATION OF [WR] CENTRAL STARS.

3.1 Physical parameters

Fig. 1 illustrates the Hertzsprung-Russell (H-R) diagram of both [WR] groups at solar metalicity ($Z = 0.01$; top panel) and a lower metalicity ($Z = 0.001$; bottom panel), in which the objects are indicated by their serial numbers in Table 1. [WRE] objects are denoted by black asterisks while [WRL] objects are indicated by blue half-filled stars. In each panel, the CS final mass isochrones, taken from [Miller Bertolami \(2016\)](#) models, were indicated using different line styles and labels.

The evolutionary age (t_{ev} in yr) isochrones were omitted for the figure clarity. It is clear from Fig. 1 that [WR] groups have different locations. [WRE] tends to be concentrated in a zone of higher T_{eff} with a spread spectrum in their luminosity (L in L_{\odot}) compared to [WRL]. From the plots, it is noticeable that both groups have a similar general trend of CS final mass distribution, despite the matalicity value. Therefore, the discussion of one of the panels is applicable to the other. In this section, we are discussing the case of low-metalicity ($Z = 0.001$); displayed in the bottom panel of Fig. 1.

For each object in Fig. 1, we estimated the final mass (M_{final} in M_{\odot}) and the evolutionary age (t_{ev} in yrs), and listed them with both T_{eff} (in K) and L (in L_{\odot}) in Table 3. The average value of each computed parameter in the table is recorded at the last row of each group; beneath their corresponding column.

The average T_{eff} (110.7 ± 5.9 kK) and L (7554 ± 1294 L_{\odot}) of [WRE]s are higher than those of [WRL]s; 35.8 ± 2.9 kK and 5223 ± 661 L_{\odot} , respectively. The location of [WRE] and [WRL] group members on the H-R diagram reveals a mean M_{final} and t_{ev} of $0.61 \pm 0.08 M_{\odot}$ and 11012 ± 3844 yr for [WRE] and $0.58 \pm 0.07 M_{\odot}$ and 7966 ± 2749 yr for [WRL] CSs, respectively. The overall mean M_{final} and t_{ev} , for the entire sample, are $0.595 \pm 0.013 M_{\odot}$ and 7966 ± 2749 yr, respectively. The mean [WR] M_{final} is higher than that of hydrogen-poor PG1159 CS class ($0.58 \pm 0.07 M_{\odot}$) while the mean [WR] t_{ev} is smaller than that of PG1159 CS class (25500 ± 5300 yr; [Ali & Alharbi 2021](#)). According to [Miller Bertolami \(2016\)](#), the average M_{final} of [WRE] and [WRL] corresponds to an initial stellar mass of $2.5 M_{\odot}$ and $1.5 M_{\odot}$, respectively. Moreover, the mean t_{ev} of [WRE] and [WRL] is 11012 ± 3844 yr and 7966 ± 2749 yr, respectively.

3.2 Kinematical parameters

The kinematical characteristics of [WR]s are analysed by investigating the Galactic velocity distribution of the stars through constructing the “Toomre diagram” and by computing their radial peculiar velocity. In this study we utilized both techniques. We calculated the space velocity components (U , V , W) and their uncertainties for early and late [WR] members following [Johnson & Soderblom \(1987\)](#); provided that the [WR] proper motion, parallax and radial velocity are known. The ‘U’ and ‘V’ components denote the Galactic center and Galactic rotation directions, respectively, whereas the component ‘W’ indicates the direction perpendicular to the Galactic disk. These components are corrected to the local standard of rest (LSR). This correction yields the (U_{LSR} , V_{LSR} , W_{LSR}) components by adding the Solar motion components (U_{\odot} , V_{\odot} , W_{\odot}) adopted to be (10, 5.5, 7.17) following [Dehnen & Binney \(1998\)](#). The corrected space rotational velocity component ‘ V_{LSR} ’ has been further corrected to the solar motion around the galactic center by adopting a solar rotational velocity ($V_R = 220$ km/s). Using (U_{LSR} , V_{LSR} , W_{LSR}), we computed the total space velocity, V_s , ($= \sqrt{U_{\text{LSR}}^2 + V_{\text{LSR}}^2 + W_{\text{LSR}}^2}$). The V_{pec} is calculated followed the procedure given by [Quireza et al. \(2007\)](#), assuming that the Galactocentric distance of the Sun is $R_{\odot} = 7.6$ kpc and the solar rotational velocity is $V_R = 220$ km/s. The uncertainty in V_s is estimated by propagating the errors in U , V , and W components. The U_{LSR} , V_{LSR} , W_{LSR} , V_s , and V_{pec} (all in km/s), for both [WRE] and [WRL] groups, are listed in Table 3.

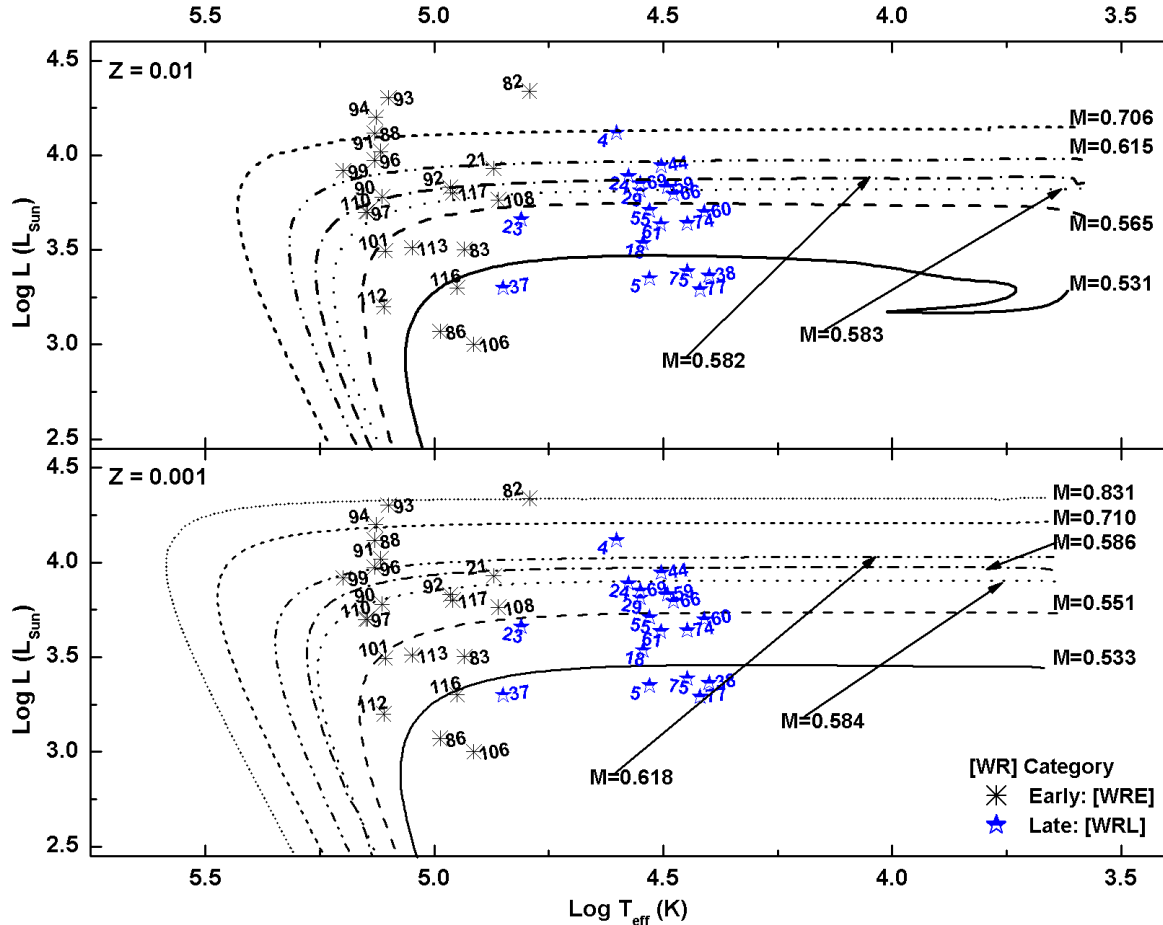


Table 3: The physical and kinematical parameters of a few number of objects in our [WR] sample organized in two groups [WRE] and [WRL]. Full data is available in the Appendix in Table A.3.

serial	PN Name	[WR] type	Physical properties				Kinematical Parameters			
			$\log T_{\text{eff}}$ (K)	$\log L$ (L_{\odot})	M_{final} (M_{\odot})	t_{ev} (yr)	$U_{\text{LSR}} \pm e$	$V_{\text{LSR}} \pm e$	$W_{\text{LSR}} \pm e$ km/s	$V_s \pm e$
[WRE]										
7	PN K 5-3	[WC 4]					168.7 ± 8.3	8.4 ± 2.0	-13.8 ± 8.5	271 ± 5.4
11	PN M 2-31	[WC 4]								89 ± 14.1
12	PN M 3-15	[WC 4]					117.5 ± 2.7	185.4 ± 52.5	-61.7 ± 14.4	137 ± 7.3
⋮			⋮	⋮					⋮	⋮
Average			0.61	11012					115 ± 25.8	51 ± 11.8
[WRL]										
1	PN H 1-62	[WC 10-11]					-68.1 ± 4.7	63.2 ± 22.0	70.1 ± 20.1	185 ± 20.2
4	PN SwSt 1	[WC 9]pec	4.60	4.12	0.65	212	3.5 ± 2.0	164.2 ± 52.3	74.1 ± 23.1	93 ± 36.4
5	PN H 1-55	[WC 11]	4.53	3.35	0.53	38139	-14.2 ± 19.3	227.5 ± 207.1	138.9 ± 58.8	140 ± 59.5
⋮			⋮	⋮					⋮	⋮
Average			0.58	7966					129 ± 29.2	59 ± 15.9

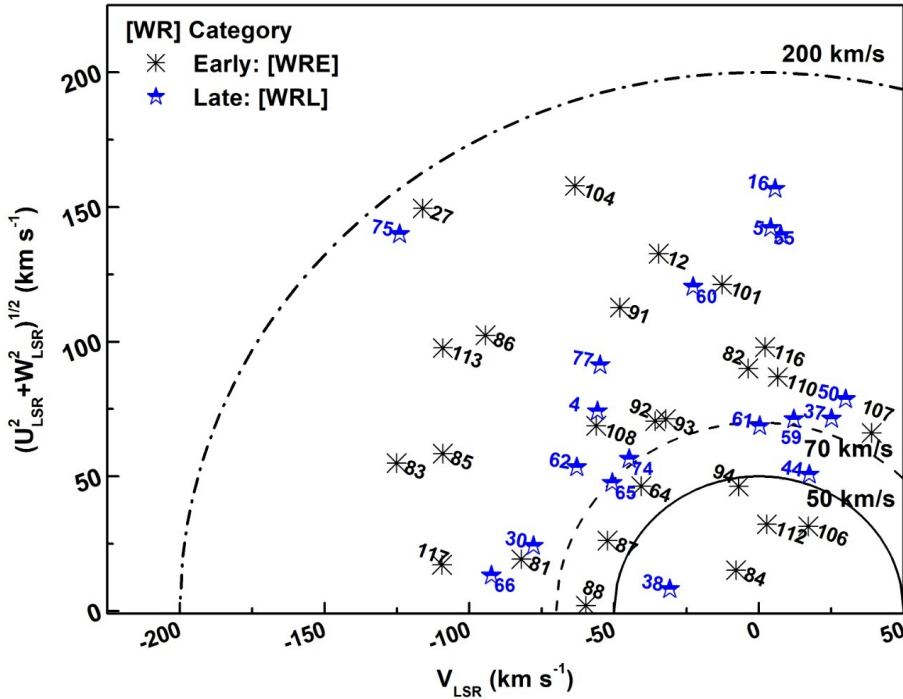


Fig. 2: The Toomre diagram for [WRE] and [WRL] group members (see figure key). The solid, dashed, and dash-dotted semi-circles refer to the constant total space velocity values at 50, 70 and 200 km/s, respectively. The error bars are omitted for the figure clarity.

3.2.1 Toomre diagram

The Toomre diagram describes the stellar distribution within the Galactic components (the thin-disk, the thick-disk, and the halo) according to their space velocity components (Bensby et al. 2003, 2010). The graph is a relation between the velocity components $\sqrt{U_{\text{LSR}}^2 + W_{\text{LSR}}^2}$ and V_{LSR} (see Fig. 2). Stellar locations within the Galactic components are defined by their total V_s as follows:

$$\text{If } V_s \text{ (km s}^{-1}\text{)} \begin{cases} < 50 & \Rightarrow \text{the Galactic thin-disc} \\ 50 \leq V_s \leq 70 & \Rightarrow \text{either the Galactic thin- or thick-disc} \\ 70 \leq V_s \leq 200 & \Rightarrow \text{the Galactic thick-disc} \\ > 200 & \Rightarrow \text{the Galactic halo} \end{cases}$$

Fig. 2 displays the Toomre diagram of [WRE] and [WRL] group members. Semi-circles indicate constant V_s at 50, 70 and 200 km/s, see labels, taken from Bensby et al. (2003, 2010). From the distribution of these objects, we noticed that 74% of the [WRE] and 80% of [WRL] members belong to the Galactic thick-disk while only 13% and 5% of the [WRE] and [WRL] members, respectively, are linked to the Galactic thin-disk. The rest of the studied sample possesses $50 < V_s < 70$ which implies that these objects reside within the overlapping region between the thin- and thick- disks. The results indicate that the majority of [WR] CS are associated with the Galactic thick-disk and there is no discrepancy between the [WRE] and [WRL] groups in terms of their location.

3.2.2 Radial peculiar velocity

[Peña et al. \(2013\)](#) analysed the V_{pec} of [WR], *WELs*, and normal CSs, where they found that most of the PNe associated with [WR] are of Peimbert type II with $V_{\text{pec}} \leq 60$ km/s and a minor fraction of type III with $V_{\text{pec}} > 60$ km/s. Additionally, they compared the kinematical properties of the [WR] and *WELs* samples and concluded that PNe associate with [WR] and those accompanied with *WEL* stars are not related.

We computed the V_{pec} for all members in the two [WR] groups and found that the mean absolute V_{pec} of [WRE] and [WRL] are 51 ± 12 and 58 ± 16 , respectively; see Table 3. The analysis showed that about 70% and 57% of [WRE] and [WRL] members, respectively, are located in the Galactic thin-disk, and hence they are of pop I, while the rest of the [WR] CSs occupies the Galactic thick-disk. Our findings are in agreement with the results of [Peña et al. \(2013\)](#), but they apparently contradict the results we obtained from the Toomre diagram. To test whether or not this contradiction is true, we performed a t-test (a statistical test aims to determine whether two processes or two groups are different) for our data. The results of the t-test revealed that the statistical significance level is very low (0.001), indicating that the two results are very close to each other and that the apparent disagreement is most likely due to the obtained uncertainties ($\sim 20\%$) in both V_s and V_{pec} .

4 CHARACTERIZING THE [WR] HOSTING NEBULAE

4.1 Physical properties

Table 4 summarizes the main physical characteristics of the PNe associated with [WR]s. The results show that nebular shells around [WRE]s possess a mean larger size ($R = 0.164 \pm 0.03$ pc) and dynamical age ($t_{\text{dyn}} = 7270 \pm 1380$ yrs) compared to those associated with [WRL] CSs: $R = 0.111 \pm 0.024$ pc and $t_{\text{dyn}} = 5350 \pm 1170$ yr.

The nebular 5 GHz emission is an essential factor for determining some physical properties such as the ionized mass (M_{ion}), optical depth (τ) and radio surface temperature (T_B). The mean value of the 5 GHz emissions unveiled that [WRE]s emit more radiation (163 ± 16 mJy) than [WRL]s (100 ± 10 mJy). We derived a mean ionized mass of $0.199 \pm 0.099 M_{\odot}$ and $0.076 \pm 0.029 M_{\odot}$ for [WRE] and [WRL], respectively. This result is consistent with the results of the initial/final mass function (e.g. [Jeffries 1997](#)) and theoretical modeling predictions (e.g. [Marigo et al. 2001](#)), where the nebular ionized mass is expected to be larger for nebulae that arise from massive progenitor stars.

The T_B parameter of PN shells can be used as a sign for their different evolutionary stages because it depends on the nebular expansion rate, mass and the exact location of the CS within the H–R plane ([Phillips 2005](#)). Our results showed that [WRL] has higher T_B (580 K) than [WRE] CSs ($T_B = 106$ K). [Cahn et al. \(1992\)](#) suggested that the T_B parameter is linked to the PN optical depth (τ), where large value of τ corresponds to low optical depth (i.e. optically thin gas) whereas small value of τ corresponds to optically thick gas. T_B increases from optically thin ($\tau > 3.13$) to optically thick ($\tau < 3.13$) nebular shells, where $\tau \sim 3.13$ indicates the transition phase from optically thick to optically thin. The mean value of τ implies that gas shells of PNe associated with [WRL] CSs are optically thicker than those hosting [WRE] CSs.

The results, in Table 4, suggest an evolutionary sequence from early to late for PNe similar to that of their [WR] stars. In that, early PNe phases are associated with higher 5 GHz emission and larger ionized mass than late PNe phases of PNe. The average values of T_B and τ reveal a tendency for PN shells around [WRE] to be optically thinner and cooler compared to PN shells around [WRL] stars.

Table 4: A portion of the physical nebular parameters surrounding the [WR]s. The PN scale height (Z), radius (R), 5GHz flux (F_{5GHz}), ionized mass (m_{ion}), optical depth (τ), and radio surface temperature (T_B). The entire table is available as Table A.4 in the Appendix.

serial	PN Name	$Z \pm e$ (pc)	$R \pm e$ (pc)	$t_{\text{dyn}} \pm e$ (yr/ 10^3)	$F_{\text{5GHz}} \pm e$ (mJy)	$m_{ion} \pm e$ (M_\odot)	τ	T_B (K)
[WRE]								
7	PN K 5-3	443 ± 97	0.143 ± 0.032	$7.00E+03 \pm 1.54E+03$				
11	PN M 2-31	383 ± 75	0.057 ± 0.011	$2.77E+03 \pm 5.44E+02$	51.0 ± 10.20	0.069 ± 0.036	2.46	252
12	PN M 3-15	391 ± 81	0.057 ± 0.012	$2.78E+03 \pm 5.75E+02$				
:	:	:	:	:	:	:	:	:
Average		370 ± 75	0.164 ± 0.030	$7.27E+03 \pm 1.38E+03$	162.5 ± 16.15	0.199 ± 0.099	3.33	106
[WRL]								
1	PN H 1-62	831 ± 290	0.076 ± 0.027	$3.72E+03 \pm 1.30E+03$				
4	PN SwSt 1	341 ± 109	0.038 ± 0.012	$2.71E+03 \pm 8.70E+02$	184.3 ± 6.00	0.035 ± 0.028	2.20	463
5	PN H 1-55	749 ± 259	0.068 ± 0.023	$3.31E+03 \pm 1.15E+03$				
:	:	:	:	:	:	:	:	:
Average		418 ± 96	0.111 ± 0.024	$5.35E+03 \pm 1.17E+03$	99.7 ± 9.97	0.076 ± 0.029	2.57	580

4.2 PN morphology, excitation class, and classification

While higher masses of PN progenitor stars are expected to give eject both bipolar (B) and elliptical (E) outflows, circular (round; R) PNe are most likely to emanate from Sun-like stars with masses $1 - 1.2 M_\odot$. The bipolar sources appear to come from far more massive stars, may be belonging to spectral type A3 or earlier (Phillips 2004). There are no differences obtained for the distribution of the three well-known morphological PN types among early and late [WR] nebulae. Both BPNe and EPNe types account for around 40% of the entire studied [WR] CS sample, whereas RPNe account for the rest of the objects ($\sim 20\%$). Table 5 summarizes the basic morphological classes, excitation class (EC), and Peimbert classification of the [WR] nebulae.

The excitation class of PNe is an important parameter that associates with few PN factors such as the nebular structure, mass, chemical abundances, and the temperature and luminosity of the CS (Gurzadian & Egikian 1991). The results reveal that [WRE] nebulae have a higher mean EC (6.9) than [WRL] nebulae (1.9). This result is consistent with the higher ionized mass, effective temperature and luminosity of the early [WR] group compared to the late [WR] group. Further, we compared the mean EC of [WRE] PNe with the non-[WR], WEL, and [WR] CSs that given by Muthumariappan & Parthasarathy (2020), where the result shows a slightly higher value than non-[WR](EC = 6.6), and greater than WEL (EC = 5.2) and [WR] (EC = 4.3) nebulae.

The results also reveal that 60% of [WRE] nebulae are of Peimbert type IIa, whereas 46% of [WRL] nebulae are of Peimbert type IIb. Moreover, Type III members account only for 12% of [WRE] and 36% of [WRL] PNe. This finding is in agreement with the idea that [WRE] nebulae originate from more massive progenitor stars than [WRL] nebulae. This result in addition to the mean scale height (Z) and V_{pec} of both [WR] groups indicate that [WRE] PNe have the tendency to belong to the Galactic thin-disk while [WRL] nebulae tend to reside in the Galactic thick-disk.

4.3 Infrared properties of [WR] nebulae

While PNe shells are mostly ionized, there is an evidence that they contain significant amounts of molecular material and dust grains. Visual extinction (A_v), especially in bipolar PNe, and the excess emission in infrared (IR) wavelengths indicate the presence of dust grains. Górný et al. (2001) examined the IR characteristics of 49 [WR] PNe, where they found that the mean T_d , increases from early to late

[WR] types. Furthermore, [Górny et al. \(2001\)](#) suggested that [WR] PNe form a homogeneous class of an evolutionary sequence, similar to their associated CSs, from compact nebulae around [WRL] stars to the more diffuse nebulae surrounding [WRE] stars.

[Muthumariappan & Parthasarathy \(2020\)](#) investigated the IR properties of ~ 100 [WR] PNe, and they found the IR characteristics of [WR] PNe are comparable to those surrounding normal and *WEL* CSs. The results showed that there is a tight anti-correlation between the age of the PN, and both the T_d and the infrared luminosity (L_{IR}). The study, also, revealed that L_{IR} of PNe has another strong anti-correlation with PN dust mass (m_d) and dust-to-gas mass ratio (m_d/m_g), in which both parameters do not change noticeably with nebular evolution time. Moreover, [Muthumariappan & Parthasarathy \(2020\)](#) found that the m_d/m_g ratio is not correlated with the age of the nebula. This result supports the previous findings of [Górny et al. \(2001\)](#).

Table 5: The excitation class (EC), Peimbert (Peim.) and morphological (mor.) types, dust temperature (T_{dust}), dust mass (m_{dust}), dust/gas mass ratio (m_{dust}/m_{gas}), and infrared luminosity (L_{IF}) of [WR]PNe. The entire table is available in the Appendix in Table A.5.

serial	PN Name	EC	Peim. Type	Mor. Type	T_{dust} (K)	$m_{dust} \pm e$ ($10^{-4} M_\odot$)	$m_{dust}/m_{gas} \pm e$ (10^{-3})	$L_{IF} \pm e$ (L_\odot)
[WRE]								
8	Hen 2-436	3.0		S	115	1.84 ± 0.75		2934 ± 1250
11	PN M 2-31	2.0		E	86	1.73 ± 0.72	2.9 ± 0.5	642 ± 340
:	:	:		:	:	:	:	:
Average		6.8			86.4	1.2 ± 0.5	3.9 ± 0.7	640.0 ± 283.6
[WRL]								
4	PN SwSt 1	8.0	IIb	S	170	0.52 ± 0.32		5825 ± 2830
5	PN H 1-55	1.0	IIb	B	73	5.42 ± 2.47		890 ± 436
:	:	:		:	:	:	:	:
Average		1.9			114.1	5.2 ± 2.4	12.0 ± 2.1	4310.6 ± 2129.6

Morphological types are: R:Round, E: Elliptical, B: Bipolar, S: Stellar

The results presented in Table 5 show an increase in the mean T_d (similar to T_B) from [WRE] to [WRL] nebulae. This finding is consistent with the results of [Górny et al. \(2001\)](#). In addition, the mean value of m_d , m_d/m_g , and L_{IR} parameters decreases from [WRL] to [WRE] PNe. This may indicate that a large fraction of dust has been destroyed by the high amount of UV radiation that emitted from the CS during the early phase of [WR] stars. All the IR mean parameters, listed in Table 5, decrease with increasing the nebular age providing further evidence for the [WR] evolutionary sequence from late to early types. The mean value for the three IR parameters for [WRL] PNe are higher than those of *WELs* and normal PN CSs.

5 ORIGIN OF [WR] CENTRAL STARS

The origin of both [WR] and *WELs* central stars in PNe is not, yet, well-understood. Different hypotheses were proposed to explain the formation of [WR] suggest that these stars originate either from the direct evolution of AGB (through a born–again scenario) or in a close binary system that goes through a common envelope phase (e.g. [Górny et al. 2001; Crowther et al. 2006](#); and references therein). Studies suggest that the occurrence of the thermal pulse (TP) in the post-AGB phase can result in an H-deficient CS (e.g. [Iben et al. 1983; Iben 1984; Herwig et al. 1999; DePew 2011](#) and [Danehkar 2014](#)). The surface abundances of H-deficient star is strongly dependent on the occurrence time of the TP beyond the AGB phase: (1) The AGB final thermal pulse (AFTP) happens at the end of the AGB when the envelope has extremely low mass and the CS has not yet entered the PN phase. This mechanism reduces the H surface abundance (15% by mass), but increases the abundance of both C and O. As a result, it cannot

account for the normal surface abundances of [WR] stars. (2) The late thermal pulse (LTP) takes place when the star advances with constant luminosity from the AGB to the white dwarf (WD) phase, and the CS has recently evolved through a PN phase. The H surface abundance remains constant during the thermal pulse. Only when the star returns to the AGB phase, the so-called born-again event occurs and a dredge-up mixing process reduces hydrogen at the surface to a few percent ($\leq 5\%$) by mass; (3) When the star is on the WD cooling track, a very late thermal pulse (VLTP) occurs. During this TP, the H surface abundance is entirely blended into the hot inner layers and the convective H–burning generates a hydrogen free star and the star is then returned to the AGB phase. The born-again scenario is suggested to be the most likely explanation for the birth of [WR] CS. Furthermore, the VLTP event has two returns to the AGB; the first returns rapidly in a few years, whilst the second takes a little longer, approximately 10^2 yr.

Unlike normal PN CSs, which are commonly of blue color, the majority of our sample (85%) tends to be red; i.e. $(BP-RP) > 0.0$; see column 4 in Table 6. To confirm this result, we collected the B and V magnitudes from [Acker et al. \(1992\)](#), where we attained the same result. Figure 3 shows the frequency distributions of $(BP-RP)$ and $(B-V)$ indices, which show that the mean values of $(BP-RP)$ and $(B-V)$ are roughly 0.85 and 0.5, respectively. We found that all members of the [WRL] category and about 83% of the [WRE] objects are red. This observed red color can be attributed to either the high interstellar reddening effect along their line-of-sights, the PNe self-reddening due to their high dust concentration content, or the visible light being dominated by its close main sequence binary companion. This astonishing result raises doubts about the commonly held belief that [WR] CS are created as a direct result of the evolved AGBs.

To examine which of these factors is responsible for the apparent reddening of the CSs, we calculated the intrinsic colour $(BP-RP)_0$ of those stars. We obtained the available reddening coefficient $E(BP-RP)$ from the eDR3 database, which only contains reddening coefficients for 21 objects. For the remaining objects, we used Equation 1 to convert $E(B-V)$, which we collected from [Frew et al. \(2016\)](#), to $E(BP-RP)$.

$$E(BP - RP) = 1.289 \times E(B - V) \quad (1)$$

Table 6: The color parameters of a sample of our [WR] entire sample. Data for the whole sample is available in Table [A.6](#) in the Appendix.

serial	PN Name	G	$(BP-RP)$	$E(BP-RP)^1$	$(B-V)$	$E(B-V)$	$E(BP-RP)^2$	$(BP-RP)_0$	Note	Ref.
1	PN H 1-62	14.4	0.77			0.49	0.63	0.14		
3	PN H 1-47	15.7	1.26		0.60	1.21	1.56	-0.30		
16	PN SB 17	17.3	2.03	0.0093				2.02		

(a) Taken from Gaia eDR3 database, (2) Computed using Eq. 1 (see text).

The results revealed that 61 of the studied 92 [WR]s are intrinsically blue (66%) while just 34% (31 items) are red. An additional study was carried out on objects with intrinsic red colour to determine whether the reddening is caused by internal (self-) extinction or close binarity. Only 11 of the objects in Table 6 are close binaries, denoted by the acronym CB. Of this set, we found that WR 72 is the only intrinsically red PN. Unfortunately, we lack a tool to confirm whether the reddening of this star is due to its binarity or the self-extinction of its host nebula. For the rest of the sample, the observed reddening might be attributed to the PN internal (self-) extinction.

This argument is supported by previous studies (e.g. [Muthumariappan & Parthasarathy 2020](#)) and the analysis of the PNe infrared properties (e.g., m_d , m_d/m_g , L_{IR} and infrared excess (IRE)), in Section 4.3, which showed that the dust content of [WR] nebulae are $\sim 3-4$ times the non-[WR] nebulae. We found that the dust content in the [WRL] PNe is larger than that in [WRE] group (see Table 5). Moreover, the dust parameters, m_d , m_d/m_g , and L_{IR} , of PNe associated with [WRL] CSs are ~ 4.3 , 4.0, and 6.7 times those values for PNe belong to the [WRE] class, respectively. As a result, a plausible explanation for the observed reddening in this subset of [WR]s (30 objects in our sample) is the internal dust extinction of their hosting PNe.

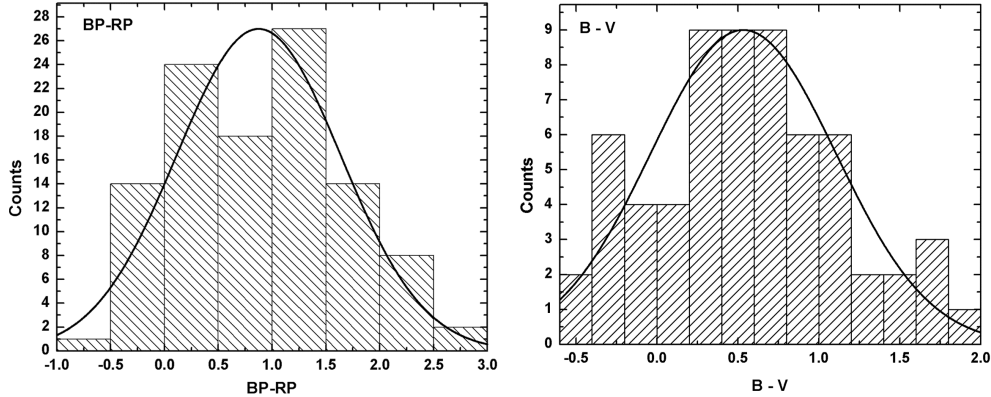


Fig. 3: A histogram represents the observed color distribution of our sources. left: (BP-BR) from Gaia eDR3 database, right: (B-V) taken from [Acker et al. \(1992\)](#).

Based on the discussion above, we may infer that, for the studied sample, the key player in the apparent reddening of [WR]s is the ISE (66%), followed by the internal extinction of the hosting PNe (32%), while the close binarity has no influence.

6 CONCLUSIONS

We analysed a sample of 117 [WR] PNe to investigate the physical and kinematical characteristics of both the [WR] stars and their associated nebulae. In a decreasing order of the T_{eff} of the [WR] CS, the sample was divided into two groups; early [WRE] and late [WRL]. The location of [WRE] and [WRL] members on the H-R diagram (Fig. 1) indicates that they have average M_{final} of $0.61 \pm 0.09 M_{\odot}$ and $0.58 \pm 0.07 M_{\odot}$ and a mean t_{ev} of $11.0 \pm 3.7 \times 10^3$ yr and $7.9 \pm 2.7 \times 10^3$ yr, respectively. Generally, [WR] CS are of a slightly higher final mass ($0.595 \pm 0.08 M_{\odot}$) than that of hydrogen poor PG1159 class ($0.58 \pm 0.08 M_{\odot}$), but of a smaller t_{ev} ($9.6 \pm 2.4 \times 10^3$ yr) than that of their peer PG1159 class ($25.5 \pm 5.3 \times 10^3$ yr; [Ali & Alharbi 2021](#)). The computed mean T_{eff} , L and t_{dyn} for [WRE] are 110.7 ± 5.9 kK, $7554 \pm 1294 L_{\odot}$ and 7270 ± 1380 yr while for [WRL] CSs are 35.8 ± 2.9 kK, $5223 \pm 661 L_{\odot}$ and 5350 ± 1170 yr, respectively.

The mean t_{dyn} of the entire [WR] sample ($= 7270 \pm 1380$ yr) is smaller than the mean t_{ev} (11012 ± 3849 yr). We may conclude that the computed t_{dyn} , in the current study, are questionable due to the lack of V_{exp} for a large number of [WR]PNe, in addition to, the assumption of constant velocity during the nebular evolution that we adopted.

While there was no obvious discrimination in nebular shape between [WRE] and [WRL] members, [WRE] PNe had a greater EC than [WRL] objects. We found that [WRE] PNe are mostly of Peimbert types IIa and IIb whereas [WRL] PNe are dominated by IIb and III types. This result and the mean Z and V_{pec} parameters imply that [WRE] PNe belong to the Galactic thin-disk while [WRL] PNe mostly belong to the Galactic thick-disk. In light of the nebular infrared analysis, we obtained higher mean values for the parameters (m_d , m_d/m_g , and L_{IR}) in [WRL] than in [WRE] group.

Finally, our data analyses showed that the interstellar extinction is responsible for two-thirds of the red apparent color obtained in the vast majority of [WR] CSs, whereas self-extinction contributed the remaining one-third.

Acknowledgements The authors would like to thank the reviewer for the constructive comments that improved the original manuscript. This work has made use of data from the European Space Agency (ESA) mission Gaia, processed by the Gaia Data Processing and Analysis Consortium(DPAC). This research has made use of the SIMBAD database, operated at CDS, Strasbourg, France.

References

- Acker, A., Marcout, J., Ochsenbein, F., et al. 1992, The Strasbourg-ESO Catalogue of Galactic Planetary Nebulae. Parts I, II. (European Southern Observatory, Garching (Germany), 1992, 1047 p., ISBN 3-923524-41-2)
- Acker, A., & Neiner, C. 2003, *A&A*, 403, 659
- Adam, C., & Mugrauer, M. 2014, *MNRAS*, 444, 3459
- Ali, A., & Alharbi, W. R. 2021, *Research in Astronomy and Astrophysics*, 21, 151
- Ali, A., & Dopita, M. A. 2019, *MNRAS*, 484, 3251
- Ali, A., Dopita, M. A., Basurah, H. M., et al. 2016, *MNRAS*, 462, 1393
- Aller, A., Lillo-Box, J., Jones, D., Miranda, L. F., & Barceló Forteza, S. 2020, *A&A*, 635, A128
- Barlow, M. J., & Hummer, D. G. 1982, in *Wolf-Rayet Stars: Observations, Physics, Evolution*, ed. C. W. H. De Loore & A. J. Willis, Vol. 99, 387
- Basurah, H. M., Ali, A., Dopita, M. A., et al. 2016, *MNRAS*, 458, 2694
- Beals, C. S. 1938, *IAU Trans.*, 6, 248
- Bensby, T., Feltzing, S., & Lundström, I. 2003, *A&A*, 410, 527
- Bensby, T., Feltzing, S., Johnson, J. A., et al. 2010, in *IAU Symposium*, Vol. 265, Chemical Abundances in the Universe: Connecting First Stars to Planets, ed. K. Cunha, M. Spite, & B. Barbuy, 346
- Cahn, J. H., Kaler, J. B., & Stanghellini, L. 1992, *A&AS*, 94, 399
- Chornay, N., & Walton, N. A. 2020, *A&A*, 638, A103
- Chornay, N., Walton, N. A., Jones, D., et al. 2021, *A&A*, 648, A95
- Crowther, P. A., De Marco, O., & Barlow, M. J. 1998, *MNRAS*, 296, 367
- Crowther, P. A., Morris, P. W., & Smith, J. D. 2006, *ApJ*, 636, 1033
- Danehkar, A. 2014, *Evolution of Planetary Nebulae with WR-type Central Stars*, PhD thesis, Macquarie University, Australia
- Danehkar, A. 2021, *ApJS*, 257, 58
- Dehnen, W., & Binney, J. J. 1998, *MNRAS*, 298, 387
- DePew, K. D. 2011, *On the Origin and Evolution of Wolf-Rayet Central Stars of Planetary Nebulae*, PhD thesis, Department of Physics and Astronomy, Macquarie University, Australia
- DePew, K., Parker, Q. A., Miszalski, B., et al. 2011, *MNRAS*, 414, 2812
- Durand, S., Acker, A., & Zijlstra, A. 1998, *A&AS*, 132, 13
- Frew, D. J., Parker, Q. A., & Bojičić, I. S. 2016, *MNRAS*, 455, 1459
- Gaia Collaboration. 2020, *VizieR Online Data Catalog*, I/350
- Gaia Collaboration, Brown, A. G. A., Vallenari, A., et al. 2018, *A&A*, 616, A1
- Girard, P., Köppen, J., & Acker, A. 2007, *A&A*, 463, 265
- Górny, S. K., Stasińska, G., Szczerba, R., & Tylenda, R. 2001, *A&A*, 377, 1007
- Gurzadian, G. A., & Egikian, A. G. 1991, *Ap&SS*, 181, 73
- Herwig, F., Blöcker, T., Langer, N., & Driebe, T. 1999, *A&A*, 349, L5
- Hiltner, W. A., & Schild, R. E. 1966, *ApJ*, 143, 770
- Iben, I., J. 1984, *ApJ*, 277, 333
- Iben, I., J., Kaler, J. B., Truran, J. W., & Renzini, A. 1983, *ApJ*, 264, 605
- Jacoby, G. H., Hillwig, T. C., & Jones, D. 2020, *MNRAS*, 498, L114
- Jeffries, R. D. 1997, *MNRAS*, 288, 585
- Johnson, D. R. H., & Soderblom, D. R. 1987, *AJ*, 93, 864
- Kingsburgh, R. L., Barlow, M. J., & Storey, P. J. 1995, *A&A*, 295, 75
- Manick, R., Miszalski, B., & McBride, V. 2015, *MNRAS*, 448, 1789
- Marigo, P., Girardi, L., Groenewegen, M. A. T., & Weiss, A. 2001, *A&A*, 378, 958
- Mendez, R. H. 1991, in *NATO Advanced Science Institutes (ASI) Series C*, Vol. 341, *NATO Advanced Science Institutes (ASI) Series C*, ed. L. Crivellari, I. Hubeny, & D. G. Hummer, 331
- Miller Bertolami, M. M. 2016, *A&A*, 588, A25
- Miszalski, B., Jones, D., Rodríguez-Gil, P., et al. 2011, *A&A*, 531, A158
- Muthumariappan, C., & Parthasarathy, M. 2020, *MNRAS*, 493, 730

- Napiwotzki, R., & Schoenberner, D. 1991, A&A, 249, L16
Peña, M., Rechy-García, J. S., & García-Rojas, J. 2013, Revista Mexicana de Astronomía y Astrofísica, 49, 87
Peimbert, M. 1978, in IAU Symposium, Vol. 76, Planetary Nebulae, ed. Y. Terzian, 215
Phillips, J. P. 2004, MNRAS, 353, 589
Phillips, J. P. 2005, MNRAS, 361, 283
Quireza, C., Rocha-Pinto, H. J., & Maciel, W. J. 2007, A&A, 475, 217
Smith, L. F., Shara, M. M., & Moffat, A. F. J. 1990, ApJ, 358, 229
Smith, L. F., Shara, M. M., & Moffat, A. F. J. 1996, MNRAS, 281, 163
Smith, L. J., Crowther, P. A., & Prinja, R. K. 1994, A&A, 281, 833
Tylenda, R., Acker, A., & Stenholm, B. 1993, A&AS, 102, 595
van der Hucht, K. A., Conti, P. S., Lundstrom, I., & Stenholm, B. 1981, Space Sci. Rev., 28, 227
Weidmann, W. A., & Gamen, R. 2011, A&A, 531, A172
Weidmann, W. A., Méndez, R. H., & Gamen, R. 2015, A&A, 579, A86
Weidmann, W. A., Mari, M. B., Schmidt, E. O., et al. 2020, A&A, 640, A10
Weinberger, R. 1989, A&AS, 78, 301
Werner, K., & Herwig, F. 2006, PASP, 118, 183
Williams, D. A. 2003, in Solid State Astrochemistry, ed. V. Pirronello, J. Krelowski, & G. Manicò, 1

Appendix A: FULL TABLES

Table A.1: A summary of the basic parameters of the studied [WR] sample.

serial	PN Name	[WR] type	Gaia eDR3 Source_ID	Galactic Coordinates l($^{\circ}$)	b($^{\circ}$)	Equatorial Coordinates R.A($^{\circ}$)	Dec.($^{\circ}$)
1	PN H 1– 62	[WC 10– 11]	4045771305065496832	0.0100	− 6.8504	273.3248	− 32.3286
2	PN M 2– 20	[WC 5– 6]	4056503259966429440	0.4132	− 1.9893	268.6055	− 29.6023
3	PN H 1– 47	[WC 11]?	4062301564840251520	1.2949	− 3.0402	270.1568	− 29.3640
4	PN SwSt 1	[WC 9]pec	4049331244394134912	1.5906	− 6.7176	274.0511	− 30.8688
5	PN H 1– 55	[WC 11]	4050131349653595392	1.7136	− 4.4554	271.8106	− 29.6902
6	PN M 1– 38	[WC 5– 6]	4050798924999155456	2.4831	− 3.7454	271.5239	− 28.6750
7	PN K 5– 3	[WC 4]	4110623760607130624	2.6087	5.5937	262.6717	− 23.7501
8	Hen 2– 436	[WC 4]	6744366945682210560	4.8712	− 22.7265	293.0279	− 34.2160
9	PN M 1– 25	[WC 5– 6]	4117211214062566528	4.9393	4.9362	264.6263	− 22.1442
10	PN MaC 1– 10	[WC 8]		5.9747	− 2.6125	272.3037	− 25.0759
11	PN M 2– 31	[WC 4]	4064771067972273920	6.0405	− 3.6205	273.3169	− 25.5015
12	PN M 3– 15	[WC 4]	4118854193637373184	6.8027	4.1606	266.3821	− 20.9671
13	PN M 2– 34	[WC]	4065541451764577408	7.8125	− 3.6999	274.3163	− 23.9816
14	NGC 6629	[WC 5– 6]	4089517157442187008	9.4070	− 5.0490	276.4269	− 23.2029
15	NGC 6578	[WC 4– 6]	4094354493205707392	10.8181	− 1.8270	274.0688	− 20.4507
16	PN SB 17	[WC 12]	4079151550306831488	11.1972	− 7.9196	280.0830	− 22.9082
17	NGC 6567	[WC 5– 6]	4094749870714268544	11.7436	− 0.6499	273.4382	− 19.0761
18	PN HuBi 1	[WC 11]		12.2194	4.9226	268.5880	− 15.9311
19	IRAS 17597– 1442	[WC 8]	4146998736283238656	14.2836	3.7959	270.6596	− 14.7008
20	IRAS 18249– 1506	[WC 4]	4103988212315867008	16.8616	− 1.7349	276.9617	− 15.0733
21	PN M 1– 60	[WC 4]	4105129677124985216	19.7950	− 4.5271	280.9089	− 13.7469
22	PMR 7	[WC 4]	4105553298336857600	21.0115	− 4.0470	281.0329	− 12.4483
23	PN M 2– 43	[WC 7– 8]	4270080782317422208	27.6787	4.2604	276.6669	− 2.7160
24	PN K 3– 18	[WC 9]	4261880968243745152	32.0147	− 3.0362	285.1451	− 2.1994
25	PN A66 58	[WC 4– 7]	4264850714784262272	37.6011	− 5.1636	289.5853	1.7832
26	PN K 3– 15	[WC 11]/VL	4311505638850116096	41.8023	4.4470	282.9231	9.9146
27	PN M 4– 13	[WC 4]	4320554035406988672	48.7715	1.9928	288.4101	14.9886
28	PN HuDo 1	[WC 11]	2021265455564470144	60.4776	1.5905	294.7171	25.0924
29	BD+30 3639	[WC 9]	2032744769234150016	64.7854	5.0194	293.6885	30.5164
30	Hen 2– 459	[WC 9]	1837452503203933184	68.3507	− 2.7382	303.4912	29.5655
31	PN A66 78	[WC]/PG 1159	1850685091269441792	81.2960	− 14.9127	323.8724	31.6960
32	IRAS 21282+5050	[WC 11]+?	2171652769005709568	93.9873	− 0.1178	322.4936	51.0668
33	PN K 3– 61	[WC 4– 6]	2177492137825896576	96.3167	2.3468	322.5032	54.4576
34	IC 5217	[WC]?	2000514441288746752	100.622	− 5.4023	335.9822	50.9668
35	PN Vy 1– 1	[WC]	419326659360627968	118.0616	− 8.6897	4.6757	53.8722
36	NGC 246	[WC]OVI	2376592910265354368	118.8631	− 74.7091	11.7639	− 11.8719
37	NGC 40	[WC 8]	537481007814722688	120.0162	9.8681	3.2542	72.5220
38	PN M 4– 18	[WC 11]	471908436438311680	146.7949	7.6012	66.4618	60.1202
39	IC 2003	[WC 3]?	218544737933650944	161.2773	− 14.8908	59.0916	33.8752
40	PN M 1– 7	[WO]/[WC 8]	3382861038566672000	189.8943	7.7927	99.3374	24.0102
41	PN A66 30	[WC]/PG 1159+?	660071056749861888	208.5575	33.2890	131.7228	17.8795
42	PHR J0723+0036	[WC 4]:	3110803653827201280	216.0961	7.4767	110.9520	0.6089
43	IRAS 06518– 1041	[WC 8]+?	3049278041153797760	222.8413	− 4.2729	103.5560	− 10.7606
44	PN M 1– 11	[WC 10– 11]	2931008523160833280	232.8366	− 4.7301	107.8196	− 19.8508
45	PMR 3	[WC 4]pec	5930814309267559552	250.2683	− 53.0402	250.2683	− 53.0402
46	WRAY 17– 23	[WC 5– 6]		270.1175	− 2.9505	134.7625	− 50.3944
47	PMR 1	[WC 4:]	5313911079687293440	272.8374	1.0324	142.1692	− 49.6122

Continued on next page

Table A.1 – *Continued from previous page*

serial	PN Name	[WR] type	Gaia eDR3 Source ID	I(°)	b(°)	R.A(°)	Dec.(°)
48	PN Pe 1– 1	[WC 5]		285.4501	1.5037	159.6151	– 56.7851
49	PHR J1134– 5243	[WO 4]/[WC 4]	5345597458614614400	291.3175	8.4058	173.6606	– 52.7256
50	PN Vo 1	[WC 10]	5208229183110454784	291.3750	– 26.2939	104.8600	– 79.6464
51	WRAY 16– 92	[WC 4]	5336037857882804736	292.8024	1.1261	172.1975	– 60.1102
52	Hen 2– 86	[WC 5– 6]	5861205190154456192	300.7107	– 2.0868	187.6270	– 64.8683
53	IRAS 12403– 6411	[WC 9]	5862586520319889920	302.0573	– 1.6091	190.8309	– 64.4670
54	PMR 6	[WC 4]	5869170013686928000	308.5470	2.4907	204.0960	– 59.8901
55	Hen 2– 99	[WC 9]	5851865148069389568	309.0027	– 4.2415	208.1278	– 66.3907
56	IRAS 13507– 6322	[WC 4]:	5864421983242008832	309.8544	– 1.5989	208.5933	– 63.6216
57	PN PM 1– 78	[WC 9]	5891918673080594176	313.9932	2.8715	214.1572	– 58.1590
58	RCW 90	[WC 5– 6]	5881321133340445696	320.9946	2.0918	226.4966	– 55.9880
59	Hen 2– 113	[WC 10]	5899715786733345536	321.0481	3.9884	224.9728	– 54.3021
60	Hen 2– 142	[WC 9]	5836438239720535040	327.1950	– 2.2044	239.9901	– 55.9258
61	CPD– 56 8032	[WC 10]	5917195002285834240	332.9152	– 9.9083	257.2539	– 56.9133
62	PN Pe 1– 7	[WC 9]	5943697901113034368	337.4742	1.6189	247.6078	– 46.0475
63	WRAY 15– 1567	[WC 10]	5977790526875496064	348.473	4.9161	253.8419	– 35.5900
64	PN H 1– 26	[WC 4– 5]	5961023459912201088	350.1428	– 3.9116	264.1246	– 39.3658
65	PN H 2– 1	[WC 11]	5978397113707361536	350.9088	4.4022	256.1511	– 33.9885
66	PN K 2– 16	[WC 11]	6033785806546839936	352.9472	11.3960	251.2044	– 28.0680
67	PN H 1– 29	[WC 4]	4041789389356118272	355.2750	– 2.5429	266.0578	– 34.2925
68	MPA J1746– 3412	[WC 10– 11]	4041758053185606656	355.5687	– 2.8668	266.5771	– 34.2103
69	PN H 1– 9	[WC 11]	4058987022459300096	355.9692	3.6263	260.3829	– 30.3469
70	PN Th 3– 13	[WC 5– 6]	4058250070404444416	356.1552	2.7649	261.3307	– 30.6784
71	PN M 1– 27	[WC 11]?	4053955824662571648	356.5312	– 2.3941	266.689	– 33.1431
72	PN H 1– 39	[WC 11]?	4043128594411861120	356.5542	– 3.9785	268.3376	– 33.9329
73	PHR J1752– 3330	[WC 11]	4043198031104721664	356.8367	– 3.6055	268.1218	– 33.5012
74	PN H 1– 43	[WC 11]	4042380857826322176	357.1835	– 4.7886	269.5602	– 33.7938
75	PN M 3– 41	[WC 11]	4059513619827242496	357.3288	3.3779	261.4993	– 29.3640
76	PN M 3– 17	[WC 11]?	4044076167334983808	359.3597	– 3.1021	269.1069	– 31.0714
77	PN M 3– 44	[WC 11]	4056355822397882880	359.3855	– 1.8139	267.8288	– 30.3981
78	PHR J1731– 2709	[WC 4]:		359.8801	3.5297	262.9492	– 27.1553
79	PN M 2– 27	[WC 4]:		359.9516	– 4.5987	270.9692	– 31.2963
80	PHR J1811– 3042	[WO 1– 2]	4049240298544263936	1.2146	– 5.6614	272.7613	– 30.7033
81	PN Cn 1– 5	[WO 4]pec	4046842607233523840	2.2913	– 9.4806	277.2985	– 31.4998
82	NGC 6369	[WO 3]	4111368477921050368	2.4320	5.8469	262.3352	– 23.7597
83	PN Hb 4	[WO 3]	4068200586367730944	3.1708	2.9285	265.4700	– 24.7023
84	PN H 1– 67	[WO 2]	4090114299627717504	9.8941	– 4.6348	276.2707	– 22.5813
85	PN M 1– 32	[WO 4]pec	4144897913181069184	11.9769	4.2336	269.0838	– 16.4846
86	PN M 3– 30	[WO 2]	4100345805124045696	17.9090	– 4.8313	280.3122	– 15.5621
87	PN M 1– 51	[WO 4]pec	4154696829542155392	20.9992	– 1.1249	278.3710	– 11.1240
88	NGC 6751	[WO 4]	4206136209740612352	29.2275	– 5.9418	286.4814	– 5.9923
89	MPA J1921+0132	[WO 3– 4]	4264619130140417664	37.7821	– 6.0274	290.4354	1.5445
90	PN PC 22	[WO 1]		51.0484	– 4.6008	295.5145	13.8437
91	NGC 6905	[WO 2]	1816547660416810880	61.4913	– 9.5714	305.5958	20.1045
92	NGC 7026	[WO 3]	2165238733564304768	89.0020	0.3752	316.5774	47.8519
93	IC 1747	[WO 4]	511904404556131200	130.2773	1.3974	29.3987	63.3218
94	NGC 1501	[WO 4]	473712872456844544	144.560	6.5510	61.7474	60.9206
95	PN Ba 1	[WO]?	50865027106484096	171.3001	– 25.8130	58.4023	19.4941
96	NGC 2371	[WO 1]	885587110718845568	189.1563	19.8431	111.3945	29.49064
97	NGC 2452	[WO 1]	5601582285451511040	243.3799	– 1.0383	116.8594	– 27.3352
98	NGC 2867	[WO 2]+?	5300450617836957312	278.1592	– 5.9363	140.3558	– 58.3113
99	PN PB 6	[WO 1]	5358679035649615232	278.8563	4.9959	153.3166	– 50.3331

Continued on next page

Table A.1 – *Continued from previous page*

serial	PN Name	[WR] type	Gaia eDR3 Source ID	I°	b°	R.A. $(^{\circ})$	Dec. $(^{\circ})$
100	PHR J1001– 6152	[WO 3]	5255947536784791936	284.2617	− 5.3293	150.3288	− 61.8669
101	Hen 2– 55	[WO 3]	5352847947540781568	286.3566	2.8185	162.1801	− 56.0527
103	BMP J1209– 5553	[WO 2]:	6075587378880414976	297.0353	6.4979	182.3712	− 55.8928
104	PN Th 2– A	[WO 3]pec	5865192362963086592	306.4137	− 0.6892	200.6408	− 63.3504
105	NGC 5189	[WO 1]+?	5863702868275424384	307.2058	− 3.4525	203.3870	− 65.9742
106	NGC 5315	[WO 4]	5851109332606802432	309.1132	− 4.3955	208.4873	− 66.5141
107	IRAS 15154– 5258	[WO 4]pec	5888049732191403904	324.0862	3.5312	229.7865	− 53.1638
108	PN PC 14	[WO 4]	5924318978646258304	336.2881	− 6.9916	256.5615	− 52.5001
109	MPA J1611– 4356	[WO 4]	5991591150152485376	336.5542	5.5092	242.8038	− 43.9394
110	WR 72	[WO 1]	6010805807350513920	341.5488	12.1049	241.6187	− 35.7534
111	PN SB 34	[WO 2]	4036440466993936640	351.5662	− 6.5868	268.0392	− 39.5375
112	PN M 2– 8	[WO 3]		352.1880	5.1252	256.3779	− 32.5356
113	PN Hf 2– 1	[WO 2]	4041465647722562688	355.4734	− 4.0974	267.8006	− 34.9234
114	PN K 6– 32	[WO 3]:	4040837482932904064	355.8986	− 4.4348	268.4163	− 34.7277
115	PHR J1753– 3428	[WO 2– 3]	4041594668305141888	356.0546	− 4.2051	268.2704	− 34.4775
116	PN M 2– 16	[WO 2– 3]		357.4824	− 3.2478	268.1432	− 32.7643
117	IC 1297	[WO 3]	6714803311390242048	358.3461	− 21.6052	289.3477	− 39.6128
118	PN A66 48	[WN 4]	4258557110213184896	29.0784	0.4542	280.6955	− 3.2215
119	PN PB 8	[WN/C]	5342835824697866880	292.4403	4.1673	173.3242	− 57.1041
120	IC 4663	[WN 3]	5955085238132418048	346.2615	− 8.2195	266.3693	− 44.9050

Table A.2: The CS proper motion (μ_{α} , μ_{δ}), parallax (ϖ), and distance (D) as well as the nebular angular radius (θ), radial velocity (V_r) and expansion velocity (V_{exp}). Distances marked with the \dagger symbol are taken from [Frew et al. \(2016\)](#).

Serial	$\mu_{\alpha} \pm \epsilon$ (mas/yr)	$\mu_{\delta} \pm \epsilon$ (mas/yr)	$\varpi \pm \epsilon$ (mas)	D $\pm \epsilon$ pc	θ (arcmin)	$V_r \pm \epsilon$ (km/s)	V_{exp} (km/s)
1	− 3.681 ± 0.040	− 3.597 ± 0.030	0.047 ± 0.034	6970 ± 2430	2.25	− 86.6 ± 4.7	20
2	2.778 ± 0.268	− 10.904 ± 0.172	− 1.930 ± 0.240	\dagger 7613 ± 1670	1.88	58.7 ± 15.0	20
3	1.323 ± 0.063	− 7.017 ± 0.044	0.091 ± 0.050	9757 ± 2139	1.25	107.5 ± 3.1	20
4	− 6.238 ± 0.133	− 1.720 ± 0.095	0.343 ± 0.110	2914 ± 934	2.70	− 17.0 ± 1.6	13.75
5	− 2.445 ± 0.779	1.415 ± 0.570	0.036 ± 0.860	9640 ± 3340	1.45	− 35.6 ± 32.6	20
6	− 0.697 ± 0.031	− 4.545 ± 0.023	0.120 ± 0.026	8335 ± 1778	1.75	− 82.8 ± 9.1	20
7	− 4.363 ± 0.539	− 9.627 ± 0.365	0.200 ± 0.337	4540 ± 1000	6.50	144.9 ± 7.1	20
8	− 0.699 ± 0.454	− 1.563 ± 0.380	− 0.521 ± 0.460		0.30		14
9	− 6.493 ± 0.166	− 6.339 ± 0.101	− 0.514 ± 0.150	\dagger 5800 ± 1271	2.00	14.1 ± 2.0	20
10							20
11			0.165 ± 0.032	6059 ± 1192	1.93	151.8 ± 2.4	20
12	1.437 ± 0.187	− 3.300 ± 0.113	0.185 ± 0.038	5391 ± 1116	2.18	97.2 ± 0.7	20
13	− 1.989 ± 0.065	− 1.302 ± 0.047	0.155 ± 0.056	6472 ± 2350	4.00	66.7 ± 9.4	20
14	− 1.090 ± 0.026	3.944 ± 0.021	0.486 ± 0.023	2058 ± 96	8.03	14.6 ± 1.3	6.25
15	− 2.263 ± 0.040	− 6.322 ± 0.032	0.371 ± 0.040	2698 ± 290	5.98	4.4 ± 1.8	20
16	− 1.767 ± 0.182	− 5.184 ± 0.128	0.885 ± 0.137	1130 ± 174	9.75	145.0 ± 29.0	20
17	− 2.693 ± 0.038	− 4.678 ± 0.033	0.350 ± 0.035	2857 ± 286	3.63	119.3 ± 0.7	27.2
18				\dagger 6880 ± 2190	7.75	43.0 ± 5.0	22
19	− 1.966 ± 0.065	− 3.326 ± 0.044	0.147 ± 0.057	6818 ± 2666	9.60		20
20	− 2.538 ± 0.357	− 6.687 ± 0.297	0.347 ± 0.340		3.90		20
21				\dagger 7196 ± 1484	1.25	93.1 ± 9.7	20
22	− 3.463 ± 0.152	− 6.650 ± 0.136	0.186 ± 0.136	9900 ± 200	7.25		20
23	− 3.320 ± 0.286	− 8.108 ± 0.258	0.161 ± 0.036	6209 ± 1400	0.80	96.4 ± 4.3	20
24	− 5.736 ± 0.433	− 5.190 ± 0.386	0.112 ± 0.012	8902 ± 913	2.01		20

Continued on next page

Table A.2 – *Continued from previous page*

Serial	$\mu_\alpha \pm e$ (mas/yr)	$\mu_\delta \pm e$ (mas/yr)	$\varpi \pm e$ (mas)	$D \pm e$ pc	θ (arcsec)	$V_r \pm e$ (km/s)	V_{exp} (km/s)
25				[†] 5680 ± 1780	20.00	70.0 ± 14.0	20
26	-1.311 ± 0.242	-2.497 ± 0.245	-0.480 ± 0.258				20
27	-3.669 ± 0.122	-7.711 ± 0.109	-0.124 ± 0.129	[†] 4577 ± 964	2.80	5.7 ± 1.0	20
28	-2.430 ± 0.051	-5.164 ± 0.072	0.006 ± 0.077	17800 ± 5410	1.03	-12.0 ± 8.0	20
29	-2.251 ± 0.028	-8.807 ± 0.028	0.618 ± 0.032	1617 ± 85	2.95	-45.9 ± 3.0	25.5
30	-2.130 ± 0.244	-9.378 ± 0.252	0.991 ± 0.300	1009 ± 306	1.25	-72.0 ± 20.0	20
31	-3.020 ± 0.024	0.428 ± 0.023	0.588 ± 0.028	1700 ± 80	59.00	17.0 ± 10.0	27
32	-3.808 ± 0.026	-2.445 ± 0.020	0.268 ± 0.019	3735 ± 258	2.63		20
33	-2.564 ± 0.117	-1.594 ± 0.116	0.108 ± 0.110	7065 ± 1441	3.50	-124.3 ± 2.4	20
34	-5.042 ± 0.077	-2.852 ± 0.069	0.189 ± 0.073	5294 ± 2033	3.50	-98.6 ± 0.4	22.75
35	0.943 ± 0.024	-0.160 ± 0.029	0.196 ± 0.031	5097 ± 815	2.60	-39.5 ± 1.3	10
36	-16.914 ± 0.095	-9.240 ± 0.085	1.799 ± 0.079	556 ± 24	121.75	-46.0 ± 4.5	39
37	-7.260 ± 0.019	-1.848 ± 0.020	0.561 ± 0.017	1782 ± 55	22.50	-15.5 ± 1.7	27.5
38	0.717 ± 0.017	-0.755 ± 0.016	0.153 ± 0.016	6544 ± 703	1.80	-17.0 ± 12.0	12.25
39	0.049 ± 0.072	-1.781 ± 0.055	0.049 ± 0.070	4211 ± 805	4.53	-15.5 ± 2.2	21.5
40	1.551 ± 1.238	-3.897 ± 0.933	1.376 ± 1.217	5337 ± 517	5.00	2.1 ± 9.2	12
41	-5.722 ± 0.035	-1.249 ± 0.026	0.452 ± 0.033	2214 ± 163	63.50		20
42	-1.059 ± 0.023	-0.063 ± 0.019	0.195 ± 0.022	5135 ± 584	35.00		20
43	-0.158 ± 0.017	0.620 ± 0.017	0.044 ± 0.016		10.80		20
44	0.240 ± 0.025	2.427 ± 0.028	0.217 ± 0.028	4600 ± 596	2.58	16.3 ± 14.1	20
45	-3.685 ± 0.085	-3.587 ± 0.053	0.099 ± 0.067		20.50		20
46				[†] 7240 ± 1416	4.50		20
47	-0.596 ± 0.056	-1.316 ± 0.057	0.411 ± 0.056	2435 ± 330	42.50		20
48				[†] 5137 ± 1121	1.50	19.8 ± 0.5	20
49	-4.779 ± 0.017	0.289 ± 0.018	0.040 ± 0.018	5080 ± 1000	19.50	-66.0 ± 23.0	20
50	-2.264 ± 0.202	8.703 ± 0.197	0.606 ± 0.169	1651 ± 460		-55.9 ± 6.0	20
51				[†] 5139 ± 1139	2.00	59.5 ± 4.0	20
52				[†] 4895 ± 1048	1.60	-7.5 ± 0.2	20
53	-5.378 ± 0.290	-0.910 ± 0.340	-0.587 ± 0.297		3.90		20
54	-5.302 ± 0.142	-2.421 ± 0.145	0.209 ± 0.198		6.00		38
55	-5.063 ± 0.009	-0.751 ± 0.014	0.207 ± 0.013	4838 ± 300	12.83	-95.0 ± 13.0	20
56	-4.714 ± 0.638	-2.846 ± 0.570	-0.017 ± 0.817		3.75		20
57	-7.847 ± 0.037	-2.270 ± 0.046	0.171 ± 0.047	5835 ± 1590	15.75		20
58	-7.067 ± 0.194	-3.003 ± 0.207	0.794 ± 0.205	1259 ± 325	2.45	44.6 ± 6.9	20
59	-4.855 ± 0.024	-0.202 ± 0.028	0.482 ± 0.027	2073 ± 114	0.70	-63.0 ± 2.0	20
60	-3.681 ± 0.040	-4.008 ± 0.035	0.273 ± 0.040	3658 ± 537	1.83	-94.5 ± 0.3	20
61	-1.461 ± 0.038	-5.982 ± 0.032	0.678 ± 0.047	1475 ± 103	1.50	-66.0 ± 10.0	20
62	-2.503 ± 0.155	-3.409 ± 0.114	-0.318 ± 0.159	[†] 4379 ± 419	2.40	-33.0 ± 9.0	20
63	-2.561 ± 0.108	-3.973 ± 0.086	-0.041 ± 0.091	[†] 8640 ± 2500	5.00		20
64	0.286 ± 0.102	-6.773 ± 0.072	0.010 ± 0.092	2020 ± 500	10.35	-36.9 ± 4.7	20
65	-4.727 ± 0.032	-1.836 ± 0.023	0.340 ± 0.025	2943 ± 217	2.00	-18.8 ± 1.9	13
66	-2.434 ± 0.027	-2.694 ± 0.019	0.175 ± 0.024	5703 ± 787	12.73	5.2 ± 12.0	20
67	-4.848 ± 0.218	-3.936 ± 0.120	-1.441 ± 0.193	[†] 10200 ± 3130	1.50	-16.9 ± 3.1	20
68	-5.047 ± 0.052	-7.259 ± 0.029	0.097 ± 0.046	10335 ± 4868			20
69	-6.690 ± 0.261	-6.305 ± 0.185	0.012 ± 0.231	[†] 5720 ± 1880	2.25	-157.6 ± 1.1	40
70				[†] 12925 ± 1386	0.83	-99.0 ± 40.0	20
71	0.139 ± 0.027	-1.181 ± 0.017	0.270 ± 0.022	3699 ± 307	3.28	-47.7 ± 0.7	8.5
72	-1.657 ± 0.051	-5.901 ± 0.033	0.030 ± 0.040	10876 ± 2362	1.00	-85.3 ± 16.0	20
73	-5.208 ± 0.038	-9.057 ± 0.025	0.039 ± 0.032		12.00		20
74	-1.386 ± 0.068	-5.898 ± 0.044	0.571 ± 0.061	1752 ± 186	1.00	49.0 ± 13.8	20

Continued on next page

Table A.2 – *Continued from previous page*

Serial	$\mu_\alpha \pm e$ (mas/yr)	$\mu_\delta \pm e$ (mas/yr)	$\varpi \pm e$ (mas)	$D \pm e$ pc	θ (arcsec)	$V_r \pm e$ (km/s)	V_{exp} (km/s)
75	0.289 ± 0.509	-5.918 ± 0.388	-1.932 ± 0.568	$\dagger 5940 \pm 1740$	2.15	-110.0 ± 16.4	20
76	-2.556 ± 0.067	0.521 ± 0.042	0.195 ± 0.062	5124 ± 1627	1.45	-32.6 ± 11.5	20
77	-1.362 ± 0.071	-1.696 ± 0.044	0.083 ± 0.062	5955 ± 1471	2.20	-99.2 ± 4.4	20
78					7.05		20
79				$\dagger 6871 \pm 1340$	1.58	147.3 ± 1.7	20
80	-2.858 ± 0.439	-0.390 ± 0.348	0.667 ± 0.421	$\dagger 5290 \pm 1000$	13.65		20
81	-2.102 ± 0.097	-4.559 ± 0.069	0.276 ± 0.086	3626 ± 1126	3.30	-30.3 ± 1.3	18
82	-0.239 ± 0.048	-0.841 ± 0.036	0.918 ± 0.049	1089 ± 59	14.75	-100.9 ± 1.6	41.6
83	-1.082 ± 0.156	-4.547 ± 0.091	0.090 ± 0.160	$\dagger 3143 \pm 621$	2.49	-61.0 ± 1.5	23
84	-8.160 ± 0.635	-5.509 ± 0.391	3.371 ± 0.551	297 ± 48	3.25	-8.3 ± 10.4	20
85	-4.372 ± 0.067	-6.535 ± 0.049	0.381 ± 0.057	2622 ± 389	4.28	-86.0 ± 7.6	15
86	-0.846 ± 0.131	-5.566 ± 0.115	0.248 ± 0.135	4797 ± 996	9.38	53.5 ± 14.0	20
87	-0.979 ± 0.161	-4.265 ± 0.138	0.339 ± 0.156	2951 ± 1362	5.93	-6.7 ± 8.8	20
88	-0.908 ± 0.044	-3.143 ± 0.036	0.291 ± 0.045	3439 ± 529	11.83	-38.9 ± 1.7	39
89	-1.813 ± 0.268	-4.351 ± 0.267	0.162 ± 0.270		3.90		15
90				$\dagger 6200 \pm 400$	8.00		20
91	-6.885 ± 0.025	-5.543 ± 0.029	0.368 ± 0.028	2717 ± 207	19.73	-8.4 ± 1.7	43.5
92	-2.748 ± 0.034	-2.904 ± 0.031	0.313 ± 0.030	3196 ± 310	14.25	-40.6 ± 0.6	45.25
93	-0.877 ± 0.026	1.019 ± 0.029	0.262 ± 0.038	3817 ± 554	6.50	-66.5 ± 3.3	27.5
94	2.143 ± 0.021	-5.261 ± 0.021	0.579 ± 0.019	1727 ± 57	26.75	36.2 ± 1.4	37
95	2.838 ± 0.183	-0.988 ± 0.132	0.744 ± 0.169	1343 ± 306	26.75	-17.0 ± 0.1	35.5
96	-1.256 ± 0.045	-7.078 ± 0.037	0.581 ± 0.046	1721 ± 136	19.88	20.8 ± 3.2	42.5
97	-2.565 ± 0.066	3.126 ± 0.079	0.342 ± 0.079	2922 ± 672	7.68	62.0 ± 2.8	31.5
98	-5.498 ± 0.066	3.036 ± 0.056	0.345 ± 0.056	2901 ± 469	7.08	18.0 ± 2.0	21.2
99	-4.734 ± 0.074	2.555 ± 0.068	0.149 ± 0.064	6706 ± 2882	5.75	58.7 ± 11.7	20
100	-7.376 ± 0.053	4.810 ± 0.044	0.268 ± 0.048	3726 ± 669	39.60		20
101	-6.287 ± 0.074	1.114 ± 0.066	0.229 ± 0.059	4372 ± 1128	9.00	-21.0 ± 0.3	20
102	-4.779 ± 0.017	0.289 ± 0.018	0.040 ± 0.018		19.50	-66.0 ± -13.2	20
103	-5.498 ± 0.234	0.905 ± 0.210	-0.059 ± 0.225	$\dagger 10930 \pm 2100$	8.00		20
104	-5.882 ± 0.031	-1.057 ± 0.037	0.161 ± 0.036	6211 ± 1406	13.03	-45.0 ± 18.0	17.5
105	-12.742 ± 0.017	-3.282 ± 0.023	0.681 ± 0.018	1469 ± 40	67.75	-8.0 ± 4.0	30.25
106	-4.679 ± 0.158	-3.486 ± 0.272	1.037 ± 0.200	964 ± 186	4.98	-34.5 ± 6.2	38.75
107	-1.042 ± 0.021	-0.341 ± 0.023	0.299 ± 0.024	3342 ± 271		-81.0 ± -16.2	20
108	-5.712 ± 0.321	-6.291 ± 0.290	0.464 ± 0.224	2155 ± 1042	3.08	-46.0 ± 7.2	20
109	-4.921 ± 0.117	-4.131 ± 0.098	0.183 ± 0.115	$\dagger 9610 \pm 1900$	8.50		20
110	-4.704 ± 0.026	-2.299 ± 0.020	0.817 ± 0.024	1225 ± 36		-92.5 ± -18.5	20
111	-2.920 ± 0.147	-8.236 ± 0.098	-0.145 ± 0.138	$\dagger 7520 \pm 1400$	10.95	-57.0 ± -11.4	20
112				$\dagger 6880 \pm 2090$	2.50	21.2 ± 1.5	20
113	-0.475 ± 0.284	-5.413 ± 0.193	0.192 ± 0.038	5219 ± 1022	8.08	-84.0 ± 4.1	20
114				$\dagger 4080 \pm 900$	10.50		20
115	-4.401 ± 0.217	-4.592 ± 0.139	0.312 ± 0.196	$\dagger 6580 \pm 1200$	6.50		20
116				$\dagger 6339 \pm 1134$	2.50	88.2 ± 4.1	20
117	-1.672 ± 0.064	-5.191 ± 0.057	0.225 ± 0.054	4437 ± 1060	5.15	10.3 ± 1.5	23.75
118	-0.190 ± 0.076	-2.658 ± 0.059	0.276 ± 0.068	3629 ± 895	20.50	41.2 ± 3.5	20
119	-7.611 ± 0.026	1.470 ± 0.023	0.170 ± 0.026	5885 ± 890	3.28	16.8 ± 4.7	8
120	-0.079 ± 0.079	-4.625 ± 0.052	0.386 ± 0.079	2593 ± 535	8.88	-52.1 ± 6.2	15

Table A.3: The effective temperature (T_{eff}) and luminosity (L) of [WR] CSs in logarithmic scale, final CS mass (M_{final}) and evolutionary age (t_{ev}). Further, the table includes the space velocity components (U, V, W) and radial peculiar velocity (V_{pec}) of the [WR] stars. The sample is arranged into two groups, Early: [WRE] and late: [WRL]. The table is limited to objects with available data.

serial	PN Name	[WR] type	Physical properties				Kinematical Parameters			
			$\log T_{\text{eff}}$ (K)	$\log L$ (L_{\odot})	M_{final} (M_{\odot})	t_{ev} (yr)	$U_{\text{LSR}} \pm \epsilon$	$V_{\text{LSR}} \pm \epsilon$	$W_{\text{LSR}} \pm \epsilon$ km/s	$V_s \pm \epsilon$
[WRE]										
7	PN K 5– 3	[WC 4]					168.7 ± 8.3	8.4 ± 2.0	-13.8 ± 8.5	271 ± 5.4
11	PN M 2 – 31	[WC 4]								127 ± 7.6
12	PN M 3 – 15	[WC 4]					117.5 ± 2.7	185.4 ± 52.5	-61.7 ± 14.4	137 ± 7.3
21	PN M 1 – 60	[WC 4]	4.87	3.93	0.59	772				47 ± 11.5
27	PN M 4 – 13	[WC 4]					149.6 ± 32.8	103.9 ± 23.2	-1.1 ± 0.4	189 ± 30.4
48	PN Pe 1 – 1	[WC 5]								31 ± 12.4
51	WRAY 16 – 92	[WC 4]								11 ± 3.1
64	PN H 1 – 26	[WC 4– 5]					-38.0 ± 4.3	-40.6 ± 11.4	-26.7 ± 7.2	$62 \pm$
67	PN H 1 – 29	[WC 4]					-23.1 ± 4.1	-57.3 ± 17.7	109.0 ± 34.7	299 ± 80.6
80	PHR J1811 – 3042	[WO 1 – 2]								48 ± 14.0
81	PN Cn 1 – 5	[WO 4]pec					-16.1 ± 1.0	137.9 ± 42.2	10.5 ± 5.3	84 ± 41.1
82	NGC 6369	[WO 3]	4.79	4.34	0.83	11	-90.0 ± 1.4	216.3 ± 7.5	-3.4 ± 0.1	90 ± 1.5
83	PN Hb 4	[WO 3]	4.93	3.42	0.55	21546	-40.3 ± 3.1	94.9 ± 35.1	-37.4 ± 13.9	137 ± 32.4
84	PN H 1 – 67	[WO 2]					4.6 ± 8.8	212.2 ± 43.7	14.5 ± 3.3	17 ± 20.3
85	PN M 1 – 32	[WO 4]pec					-57.9 ± 6.8	110.8 ± 13.8	7.9 ± 14.4	124 ± 12.6
86	PN M 3 – 30	[WO 2]	4.99	3.07	0.57	2993	95.1 ± 16.8	125.6 ± 31.1	-38.0 ± 7.5	139 ± 24.1
87	PN M 1 – 51	[WO 4]pec					24.9 ± 21.3	167.7 ± 74.9	-8.1 ± 4.0	58 ± 67.6
88	NGC 6751	[WO 4]	5.13	4.12	0.68	203	1.3 ± 0.6	160.3 ± 17.6	1.6 ± 0.5	60 ± 17.6
90	PN PC 22	[WO 1]	5.11	3.78	0.59	2601				87 ± 9.1
91	NGC 6905	[WO 2]	5.12	4.02	0.65	380	104.8 ± 8.3	172.0 ± 12.3	41.4 ± 3.1	123 ± 8.7
92	NGC 7026	[WO 3]	4.97	3.83	0.59	2094	70.1 ± 6.9	184.2 ± 2.7	7.6 ± 9.5	79 ± 6.3
93	IC 1747	[WO 4]	5.10	4.30	0.83	41	68.8 ± 3.7	187.8 ± 15.6	18.8 ± 3.3	78 ± 7.2
94	NGC 1501	[WO 4]	5.13	4.20	0.68	203	-45.6 ± 1.2	213.1 ± 23.4	-7.9 ± 0.4	47 ± 3.6
96	NGC 2371	[WO 1]	5.13	3.97	0.62	831	-11.2 ± 1.6	170.9 ± 12.8	-13.7 ± 1.6	52 ± 12.1
97	NGC 2452	[WO 1]	5.15	3.70	0.60	1410	-67.1 ± 10.0	194.5 ± 39.0	-2.0 ± 0.5	72 ± 16.7
99	PN PB 6	[WO 1]	5.20	3.92	0.62	939	-148.3 ± 67.6	139.0 ± 27.2	-4.7 ± 3.0	169 ± 60.7
101	WRAY 16 – 79	[WO 3]	5.11	3.49	0.55	8958	-117.1 ± 28.8	207.3 ± 112.8	-31.1 ± 7.9	122 ± 30.1
104	PN Th 2 – A	[WO 3]pec					-157.8 ± 31.7	156.5 ± 63.1	-0.5 ± 0.1	170 ± 37.6
106	NGC 5315	[WO 4]	4.91	3.00	0.53	51670	-31.4 ± 4.2	237.0 ± 115.3	-0.1 ± 0.0	36 ± 55.0
										33 ± 7.2

Continued on next page

Table A.3 – *Continued from previous page*

serial	PN Name	[WR] type	$\log T_{\text{eff}}$	$\log L$	M_{final}	t_{ev}	$U_{\text{LSR}} \pm e$	$V_{\text{LSR}} \pm e$	$W_{\text{LSR}} \pm e$	$V_s \pm e$	$V_{\text{pec}} \pm e$
107	IRAS 15154– 5258	[WO 4]pec					-65.8 ± 11.4	259.0 ± 73.3	7.2 ± 194.9	77 ± 42.6	24 ± 16.4
108	PN PC 14	[WO 4]	4.86	3.76	0.57	2521	-65.1 ± 15.1	163.9 ± 103.1	22.2 ± 8.1	89 ± 66.2	8 ± 14.0
109	MPA J1611– 4356	[WO 4]									
110	WR 72	[WO 1]	5.15	3.70	0.57	5210	-86.9 ± 15.5	226.6 ± 203.8	-2.4 ± 0.9	87 ± 21.8	79 ± 17.6
111	PN SB 34	[WO 2]					-96.1 ± 13.2	-69.0 ± 13.2	41.1 ± 9.8	307 ± 13.2	148 ± 37.4
112	PN M 2– 8	[WO 3]	5.11	3.20	0.55	36481	31.0 ± 2.2	222.8 ± 15.6	8.8 ± 0.6	32 ± 2.5	158 ± 41.1
113	PN Hf 2– 1	[WO 2]	5.05	3.51	0.55	36699	-87.6 ± 4.4	110.9 ± 23.5	-43.3 ± 11.1	146 ± 18.0	46 ± 7.8
115	PHR J1753– 3428	[WO 2– 3]									
116	PN M 2– 16	[WO 2– 3]	4.95	3.30	0.53	52863	97.9 ± 4.5	222.2 ± 10.3	1.3 ± 0.1	98 ± 4.5	134 ± 8.0
117	IC 1297	[WO 3]	4.96	3.80	0.57	2825	16.8 ± 4.0	110.6 ± 26.4	3.2 ± 1.1	111 ± 26.1	29 ± 3.6
Average				0.61	11012					115 ± 25.8	51 ± 11.8
[WRL]											
1	PN H 1– 62	[WC 10– 11]					-68.1 ± 4.7	63.2 ± 22.0	70.1 ± 20.1	185 ± 20.2	73 ± 3.9
4	PN SwSt 1	[WC 9]pec	4.60	4.12	0.65	212	3.5 ± 2.0	164.2 ± 52.3	74.1 ± 23.1	93 ± 36.4	10 ± 1.3
5	PN H 1– 55	[WC 11]	4.53	3.35	0.53	38139	-14.2 ± 19.3	227.5 ± 207.1	138.9 ± 58.8	140 ± 59.5	93 ± 38.1
16	PN SB 17	[WC 12]					155.8 ± 30.0	225.6 ± 161.0	-18.1 ± 3.2	157 ± 30.4	158 ± 32.5
18	PN HuBi 1	[WC 11]	4.54	3.54	0.54	11420					117 ± 53.1
23	PN M 2– 43	[WC 7– 8]	4.81	3.66	0.55	6284	216.9 ± 29.3	44.8 ± 12.7	-11.0 ± 6.0	279 ± 24.2	29 ± 30.3
24	PN K 3– 18	[WC 9]	4.58	3.89	0.59	584					
28	PN HuDo 1	[WC 11]					423.6 ± 130.7	-18.3 ± 5.4	-32.4 ± 10.5	487 ± 113.7	85 ± 29.5
29	BD+30 3639	[WC 9]	4.55	3.81	0.57	1503	52.4 ± 4.5	156.9 ± 7.0	-14.4 ± 0.7	83 ± 6.0	51 ± 2.9
30	Hen 2– 459	[WC 9]					23.5 ± 24.5	142.1 ± 32.8	-5.7 ± 2.3	82 ± 32.1	61 ± 16.8
37	NGC 40	[WC 8]	4.85	3.30	0.83	47	71.4 ± 2.2	245.1 ± 22.4	-2.3 ± 0.1	76 ± 7.7	10 ± 2.3
38	PN M 4– 18	[WC 11]	4.40	3.36	0.53	9279	6.6 ± 19.6	189.2 ± 37.0	4.9 ± 3.8	32 ± 36.0	33 ± 12.3
44	PN M 1– 11	[WC 10– 11]	4.50	3.95	0.59	534	-36.6 ± 7.6	237.4 ± 233.5	35.0 ± 5.0	54 ± 76.1	57 ± 7.4
55	WRAY 16– 139	[WC 9]	4.53	3.71	0.55	3762	-139.8 ± 9.3	224.0 ± 1703.3	26.3 ± 1.8	142 ± 49.3	50 ± 13.9
59	WRAY 15– 1269	[WC 10]	4.49	3.83	0.57	1432	-66.9 ± 1.9	232.1 ± 77.3	24.4 ± 1.7	72 ± 13.1	36 ± 2.6
60	WRAY 16– 198	[WC 9]	4.41	3.70	0.55	4129	-120.4 ± 6.9	197.3 ± 81.1	1.2 ± 0.3	123 ± 16.5	21 ± 9.5
61	CPD– 56 8032	[WC 10]	4.51	3.64	0.55	11880	-68.6 ± 7.8	220.2 ± 211.7	3.7 ± 2.2	69 ± 7.8	47 ± 9.6
62	PN Pe 1– 7	[WC 9]					-53.3 ± 7.5	157.1 ± 20.3	-3.8 ± 1.1	82 ± 16.2	60 ± 9.3
65	PN H 2– 1	[WC 11]					-20.1 ± 1.4	169.3 ± 13.2	43.1 ± 3.3	70 ± 9.8	3 ± 2.3
66	PN K 2– 16	[WC 11]	4.48	3.79	0.57	1404	2.8 ± 4.5	127.6 ± 17.6	12.9 ± 5.5	93 ± 17.5	69 ± 19.7
69	PN H 1– 9	[WC 11]	4.55	3.85	0.57	120	-172.7 ± 5.3	-101.9 ± 22.6	72.5 ± 20.1	372 ± 20.1	53 ± 43.7
74	PN H 1– 43	[WC 11]	4.45	3.64	0.55	11256	55.3 ± 16.8	175.2 ± 18.0	-11.5 ± 1.3	72 ± 17.0	54 ± 14.5
75	PN M 3– 41	[WC 11]	4.45	3.39	0.53	33434	-100.4 ± 14.9	95.9 ± 30.4	-97.5 ± 29.8	187 ± 26.7	71 ± 17.7

Continued on next page

Table A.3 – *Continued from previous page*

serial	PN Name	[WR] type	$\log T_{\text{eff}}$	$\log L$	M_{final}	t_{ev}	$U_{\text{LSR}} \pm e$	$V_{\text{LSR}} \pm e$	$W_{\text{LSR}} \pm e$	$V_s \pm e$	$V_{\text{pec}} \pm e$
77	PN M 3–44	[WC 11]	4.42	3.29			-89.0 ± 4.0	165.2 ± 41.3	20.0 ± 4.4	106 ± 21.5	75 ± 4.1
	Average									129 ± 29.2	59 ± 15.9

Table A.4: The physical nebular parameters surrounding the [WR]s. The PN scale height (Z), radius (R), 5GHz flux ($F_{5\text{GHz}}$), ionized mass (m_{ion}), optical depth (τ), and radio surface temperature (T_B).

serial	PN Name	$Z \pm e$ (pc)	$R \pm e$ (pc)	$f_{\text{dyn}} \pm e$ (yr/ 10^3)	$F_{5\text{GHz}} \pm e$ (mJy)	$m_{ion} \pm e$ (M_\odot)	τ	T_B (K)
[WRE]								
7	PN K 5– 3	443 ± 97	0.143 ± 0.032	7.00E+03 ± 1.54E+03				
11	PN M 2– 31	383 ± 75	0.057 ± 0.011	2.77E+03 ± 5.44E+02	51.0 ± 10.20	0.069 ± 0.036	2.46	252
12	PN M 3– 15	391 ± 81	0.057 ± 0.012	2.78E+03 ± 5.75E+02				
21	PN M 1– 60	568 ± 117	0.044 ± 0.009	2.13E+03 ± 4.40E+02	50.0 ± 11.00	0.055 ± 0.030	2.10	586
22	PMR 7	699 ± 14	0.348 ± 0.007	1.70E+04 ± 3.44E+02				
27	PN M 4– 13	159 ± 34	0.062 ± 0.013	3.04E+03 ± 6.40E+02	69.0 ± 13.80	0.070 ± 0.038	2.66	161
48	PN Pe 1– 1	135 ± 29	0.037 ± 0.008	1.83E+03 ± 3.99E+02				
51	WRAY 16– 92	101 ± 22	0.050 ± 0.011	2.44E+03 ± 5.40E+02	41.0 ± 12.00	0.043 ± 0.025	2.59	188
64	PN H 1– 26	138 ± 34	0.101 ± 0.025	4.96E+03 ± 1.23E+03				
67	PN H 1– 29	453 ± 139	0.074 ± 0.023	3.63E+03 ± 1.11E+03				
80	PHR J1811– 3042	522 ± 99	0.350 ± 0.066	1.71E+04 ± 3.24E+03				
81	PN Cn 1– 5	597 ± 185	0.058 ± 0.018	3.15E+03 ± 9.79E+02	44.0 ± 4.00	0.040 ± 0.032	3.00	74
82	NGC 6369	111 ± 6	0.078 ± 0.004	1.83E+03 ± 9.85E+01	2002.0 ± 65.00	0.126 ± 0.025	2.64	168
83	PN Hb 4	161 ± 32	0.038 ± 0.007	1.61E+03 ± 3.19E+02	167.6 ± 16.00	0.036 ± 0.018	2.17	495
84	PN H 1– 67	24 ± 4	0.005 ± 0.001	2.29E+02 ± 3.73E+01	11.2 ± 1.00	0.000 ± 0.000	3.58	19
85	PN M 1– 32	194 ± 29	0.054 ± 0.008	3.54E+03 ± 5.26E+02	62.5 ± 8.00	0.031 ± 0.012	3.07	63
86	PN M 3– 30	404 ± 84	0.218 ± 0.045	1.07E+04 ± 2.21E+03	7.0 ± 1.00	0.153 ± 0.084	4.70	1
87	PN M 1– 51	58 ± 27	0.085 ± 0.039	4.15E+03 ± 1.91E+03	319.0 ± 32.00	0.154 ± 0.179	2.64	166
88	NGC 6751	356 ± 55	0.197 ± 0.030	4.95E+03 ± 7.61E+02	63.0 ± 11.00	0.283 ± 0.117	3.95	8
90	PN PC 22	497 ± 32	0.240 ± 0.016	1.18E+04 ± 7.59E+02	11.0 ± 10.00	0.288 ± 0.076	4.37	3
91	NGC 6905	452 ± 34	0.260 ± 0.020	5.84E+03 ± 4.44E+02	62.0 ± 11.00	0.336 ± 0.082	4.40	3
92	NGC 7026	21 ± 2	0.221 ± 0.021	4.77E+03 ± 4.63E+02	277.0 ± 77.00	0.655 ± 0.187	3.47	25
93	IC 1747	93 ± 14	0.120 ± 0.017	4.28E+03 ± 6.21E+02	126.7 ± 24.00	0.213 ± 0.084	3.13	55
94	NGC 1501	197 ± 7	0.224 ± 0.007	5.92E+03 ± 1.96E+02	224.0 ± 44.80	0.325 ± 0.056	4.11	6
96	NGC 2371	584 ± 46	0.166 ± 0.013	3.82E+03 ± 3.02E+02	88.5 ± 18.00	0.130 ± 0.032	4.25	4
97	NGC 2452	53 ± 12	0.109 ± 0.025	3.38E+03 ± 7.76E+02	55.0 ± 9.00	0.092 ± 0.055	3.63	17
99	PN PB 6	584 ± 251	0.187 ± 0.080	9.14E+03 ± 3.93E+03	30.0 ± 11.00	0.352 ± 0.383	3.64	17
100	PHR J1001– 6152	346 ± 62	0.715 ± 0.128	3.50E+04 ± 6.28E+03				
101	WRAY 16– 79	215 ± 55	0.191 ± 0.049	9.33E+03 ± 2.41E+03				
104	PN Th 2– A	75 ± 17	0.392 ± 0.089	2.19E+04 ± 4.96E+03	60.0 ± 10.00	1.402 ± 0.821	4.05	6
106	NGC 5315	74 ± 14	0.023 ± 0.004	5.87E+02 ± 1.13E+02	415.0 ± 10.00	0.008 ± 0.004	2.38	307
107	IRAS 15154– 5258	206 ± 17						
108	PN PC 14	262 ± 127	0.032 ± 0.016	1.57E+03 ± 7.60E+02	30.0 ± 10.00	0.008 ± 0.010	3.10	58
109	MPA J1611– 4356	923 ± 182	0.396 ± 0.078	1.94E+04 ± 3.83E+03				
111	PN SB 34	863 ± 161	0.399 ± 0.074	1.95E+04 ± 3.64E+03				
112	PN M 2– 8	615 ± 187	0.083 ± 0.025	4.08E+03 ± 1.24E+03	18.0 ± 3.60	0.083 ± 0.065	3.14	53
113	PN Hf 2– 1	373 ± 73	0.204 ± 0.040	9.99E+03 ± 1.96E+03	9.0 ± 1.10	0.172 ± 0.088	4.46	3
115	PHR J1753– 3428	482 ± 88	0.207 ± 0.038	1.01E+04 ± 1.85E+03				
116	PN M 2– 16	359 ± 64	0.077 ± 0.014	3.76E+03 ± 6.72E+02	25.0 ± 3.00	0.080 ± 0.038	3.00	73
117	IC 1297	1634 ± 390	0.111 ± 0.026	4.56E+03 ± 1.09E+03	69.0 ± 8.60	0.161 ± 0.099	3.19	48
Average		370 ± 75	0.164 ± 0.030	7.27E+03 ± 1.38E+03	162.5 ± 16.15	0.199 ± 0.099	3.33	106
[WRL]								
1	PN H 1– 62	831 ± 290	0.076 ± 0.027	3.72E+03 ± 1.30E+03				
4	PN SwSt 1	341 ± 109	0.038 ± 0.012	2.71E+03 ± 8.70E+02	184.3 ± 6.00	0.035 ± 0.028	2.20	463
5	PN H 1– 55	749 ± 259	0.068 ± 0.023	3.31E+03 ± 1.15E+03				
16	PN SB 17	156 ± 24	0.053 ± 0.008	2.61E+03 ± 4.03E+02				
18	PN HuBi 1	590 ± 188	0.259 ± 0.082	1.15E+04 ± 3.66E+03				

Continued on next page

Table A.4 – *Continued from previous page*

serial	PN Name	$Z \pm e$ (pc)	$R \pm e$ (pc)	$t_{\text{dyn}} \pm e$ (yr/ 10^3)	$5\text{GHz} \pm e$ (mJy)	$m_{ion} \pm e$	τ	T_B (K)
19	IRAS 17597– 1442	451 ± 177	0.317 ± 0.124	$1.55E+04 \pm 6.07E+03$				
23	PN M 2– 43	461 ± 104	0.024 ± 0.005	$1.18E+03 \pm 2.66E+02$				
24	PN K 3– 18	472 ± 48	0.087 ± 0.009	$4.24E+03 \pm 4.35E+02$	12.3 ± 2.00	0.095 ± 0.029	3.12	56
28	PN HuDo 1	494 ± 150	0.088 ± 0.027	$4.33E+03 \pm 1.32E+03$				
29	BD+30 3639	141 ± 7	0.023 ± 0.001	$8.87E+02 \pm 4.66E+01$	580.3 ± 38.00	0.016 ± 0.003	1.78	1220
30	Hen 2– 459	48 ± 15	0.006 ± 0.002	$2.99E+02 \pm 9.06E+01$	61.0 ± 12.00			
37	NGC 40	305 ± 9	0.194 ± 0.006	$6.92E+03 \pm 2.12E+02$				
38	PN M 4– 18	866 ± 93	0.057 ± 0.006	$4.56E+03 \pm 4.90E+02$	20.1 ± 2.30	0.048 ± 0.015	2.81	114
44	PN M 1– 11	379 ± 49	0.057 ± 0.007	$2.81E+03 \pm 3.64E+02$	116.0 ± 21.00	0.081 ± 0.029	2.36	320
50	PN Vo 1	731 ± 204						
55	WRAY 16– 139	358 ± 22	0.301 ± 0.019	$1.47E+04 \pm 9.14E+02$	18.0 ± 5.00	0.402 ± 0.090	4.56	2
57	PN PM 1– 78	292 ± 80	0.446 ± 0.121	$2.18E+04 \pm 5.94E+03$				
59	WRAY 15– 1269	144 ± 8	0.007 ± 0.000	$3.44E+02 \pm 1.89E+01$	115.0 ± 12.00	0.002 ± 0.000	1.23	4295
60	WRAY 16– 198	141 ± 21	0.032 ± 0.005	$1.58E+03 \pm 2.32E+02$	65.0 ± 4.00	0.020 ± 0.008	2.31	357
61	CPD– 56 8032	254 ± 18	0.011 ± 0.001	$5.25E+02 \pm 3.65E+01$				
62	PN Pe 1– 7	124 ± 12	0.051 ± 0.005	$2.49E+03 \pm 2.38E+02$	119.0 ± 10.00	0.065 ± 0.018	2.29	378
63	WRAY 15– 1567	740 ± 214	0.209 ± 0.061	$1.02E+04 \pm 2.96E+03$				
65	PN H 2– 1	226 ± 17	0.029 ± 0.002	$2.15E+03 \pm 1.58E+02$	63.0 ± 6.00	0.013 ± 0.003	2.40	288
66	PN K 2– 16	1127 ± 156	0.352 ± 0.049	$1.72E+04 \pm 2.38E+03$				
68	MPA J1746– 3412	517 ± 243						
69	PN H 1– 9	503 ± 107	0.087 ± 0.019	$2.12E+03 \pm 4.53E+02$	25.0 ± 3.00	0.120 ± 0.067	2.91	90
74	PN H 1– 43	146 ± 16	0.008 ± 0.001	$4.16E+02 \pm 4.41E+01$	6.0 ± 1.20	0.000 ± 0.000	2.82	110
75	PN M 3– 41	350 ± 103	0.062 ± 0.018	$3.03E+03 \pm 8.87E+02$	75.0 ± 20.00	0.094 ± 0.070	2.39	297
77	PN M 3– 44	188 ± 47	0.064 ± 0.016	$3.11E+03 \pm 7.68E+02$	35.0 ± 7.00	0.067 ± 0.043	2.74	132
Average		418 ± 96	0.111 ± 0.024	$5.35E+03 \pm 1.17E+03$	99.7 ± 9.97	0.076 ± 0.029	2.57	580

Table A.5: The excitation class (EC), Peimbert (Peim.) and morphological (mor.) types, dust temperature (T_{dust}), dust mass (m_{dust}), dust/gas mass ratio ($m_{\text{dust}}/m_{\text{gas}}$), and infrared luminosity (L_{IF}) of [WR]PNe.

serial	PN Name	EC	Peim. Type	Mor. Type	T_{dust} (K)	$m_{\text{dust}} \pm e$ ($10^{-4} M_{\odot}$)	$m_{\text{dust}}/m_{\text{gas}} \pm e$ (10^{-3})	$L_{\text{IF}} \pm e$ (L_{\odot})
[WRE]								
7	PN K 5– 3	11.0	IIb	R				
8	Hen 2– 436	3.0		S	115	1.84 ± 0.75		2934 ± 1250
11	PN M 2– 31	2.0		E	86	1.73 ± 0.72	2.9 ± 0.5	642 ± 340
12	PN M 3– 15	6.0	IIa	B	89	2.01 ± 0.89	2.6 ± 0.5	888 ± 385
20	IRAS 18249– 1506			R	77			
21	PN M 1– 60	4.0	IIa	B	87	3.41 ± 0.55	4.9 ± 0.6	1348 ± 741
22	PMR 7			E				
27	PN M 4– 13			B	85	0.91 ± 0.45	9.2 ± 1.5	321 ± 143
48	PN Pe 1– 1	4.0	IIb	B	114	1.49 ± 0.55	3.2 ± 0.5	2270 ± 1250
51	WRAY 16– 92	7.0		E				
54	PMR 6			E				
64	PN H 1– 26			B				
67	PN H 1– 29	4.0	IIa	S				
80	PHR J1811– 3042			Es	76	1.00 ± 0.41		201 ± 80
81	PN Cn 1– 5	1.0	IIb	B	92	1.75 ± 0.73	6.0 ± 1.0	914 ± 368
82	NGC 6369	4.0	III	E	85	0.85 ± 0.37	3.1 ± 0.6	300 ± 131
83	PN Hb 4	7.0	IIa	B	81	1.89 ± 0.82	5.0 ± 0.9	522 ± 221

Continued on next page

Table A.5 – *Continued from previous page*

serial	PN Name	EC	Peim. Type	Mor. type	T _{dust} (K)	m _{dust} ± e (M _⊕)	m _{dust/m_{gas}} ± e	L _{IR} ± e (L _⊕)
84	PN H 1– 67	10.0	IV	E	84	0.61 ± 0.39	1.1 ± 0.2	202 ± 110
85	PN M 1– 32	2.0	IIa	E	94	1.60 ± 0.57	2.1 ± 0.5	929 ± 418
86	PN M 3– 30	11.0	IIa	R	77	0.67 ± 0.35	8.7 ± 1.5	145 ± 64
87	PN M 1– 51	2.0	IIa	B	90	1.33 ± 0.63	2.5 ± 0.5	625 ± 287
88	NGC 6751	9.0	IIa	E	91	1.10 ± 0.47	5.7 ± 1.0	547 ± 226
89	MPA J1921+0132			R				
90	PN PC 22	6.0		B				
91	NGC 6905	11.0	IIb	B	89	0.29 ± 0.11	0.9 ± 0.2	126 ± 51
92	NGC 7026	9.0	IIa	B	78	1.47 ± 0.63	4.8 ± 0.9	336 ± 137
93	IC 1747	9.0	IIa	E	79	0.92 ± 0.41	3.4 ± 0.5	223 ± 102
94	NGC 1501	10.0	IIb	E	75	0.32 ± 0.15	1.5 ± 0.3	60 ± 26
96	NGC 2371	12.0	IIa	B	87	0.39 ± 0.17	1.1 ± 0.2	155 ± 64
97	NGC 2452	10.0	IIa	E	90	0.58 ± 0.23	2.6 ± 0.4	272 ± 109
99	PN PB 6	5.0	IIa	E	104	0.81 ± 0.35	2.5 ± 0.4	774 ± 329
100	PHR J1001– 6152			R				
101	WRAY 16– 79			R	97	0.22 ± 0.11	0.7 ± 0.1	149 ± 72
102	PHR J1134– 5243			E	73		7.1 ± 1.4	1161 ±
104	PN Th 2– A			IIa	R	84	0.34 ± 0.15	1.1 ± 0.2
106	NGC 5315	2.0	I	B	94	2.44 ± 1.00	14.0 ± 2.4	1422 ± 584
107	IRAS 15154– 5258			E				
108	PN PC 14	6.0	III	B				
109	MPA J1611– 4356			R				
110	WR 72				63			
111	PN SB 34			R	73	3.23 ± 1.30		530 ± 219
112	PN M 2– 8	9.0	III	E				
113	PN Hf 2– 1	11.0		B	89	0.47 ± 0.20	1.9 ± 0.3	206 ± 87
115	PHR J1753– 3428			E				
116	PN M 2– 16	7.0	IIa	B				
117	IC 1297	9.0	IIb	B	81	0.89 ± 0.37	2.3 ± 0.4	245 ± 100
	Average	6.8			86.4	1.2 ± 0.5	3.9 ± 0.7	640.0 ± 283.6
	[WRL]							
1	PN H 1– 62			R				
4	PN SwSt 1	8.0	IIb	S	170	0.52 ± 0.32		5825 ± 2830
5	PN H 1– 55	1.0	IIb	B	73	5.42 ± 2.47		890 ± 436
10	PN MaC 1– 10			B				
16	PN SB 17			E	99	1.40 ± 0.62		1055 ± 447
18	PN HuBi 1			R	99	4.30 ± 1.90		3239 ± 1458
19	IRAS 17597– 1442			B				
23	PN M 2– 43	2.0	IIb	E	140	2.23 ± 1.10	3.2 ± 0.6	9499 ± 4788
24	PN K 3– 18			S				
28	PN HuDo 1			S	110	8.96 ± 3.90		
29	BD+30 3639			E	111	3.66 ± 1.50	5.4 ± 0.9	4884 ± 1960
30	Hen 2– 459			III	B	97	13.00 ± 8.50	8.8 ± 1.4
37	NGC 40	1.0	IIa	B	101	0.68 ± 0.28	1.1 ± 0.2	564 ± 226
38	PN M 4– 18			E	136	0.68 ± 0.28	0.8 ± 0.1	2516 ± 1042
44	PN M 1– 11			IIa	E			
50	PN Vo 1							
53	IRAS 12403– 6411			S				
55	WRAY 16– 139	3.0	III	E	94	2.44 ± 1.00	14.0 ± 2.4	1422 ± 584
57	PN PM 1– 78			R	82			
59	WRAY 15– 1269	1.0		B	120	39.00 ± 16.00	44.8 ± 7.7	9700 ± 5300

Continued on next page

Table A.5 – *Continued from previous page*

serial	PN Name	EC	Peim. Type	Mor. type	T _{dust} (K)	m _{dust} ± e (M _⊕)	m _{dust/m_{gas}} ± e	L _{IR} ± e (L _⊕)
60	WRAY 16– 198	1.0	IIb	E	126	1.11 ± 0.53	19.6 ± 3.5	2767 ± 1298
61	CPD– 56 8032			B	107			
62	PN Pe 1– 7	1.0	III	B	99			
63	WRAY 15– 1567			S	108	0.37 ± 0.16		
65	PN H 2– 1	1.0	IIb	B	124	0.75 ± 0.32	1.1 ± 0.2	1728 ± 737
66	PN K 2– 16			E	106	5.30 ± 2.20		5618 ± 2336
68	MPA J1746– 3412			S				
69	PN H 1– 9	1.0		S	215	0.11 ± 0.06		4165 ± 1936
73	PHR J1752– 3330			E				
74	PN H 1– 43	1.0	III	B	102	7.20 ± 3.40	21.0 ± 4.0	6263 ± 2926
75	PN M 3– 41			S	92	0.78 ± 0.33		
77	PN M 3– 44			B				
	Average	1.9			114.1	5.2 ± 2.4	12.0 ± 2.1	4310.6 ± 2129.6

Morphological types are: R:Round, E: Elliptical, B: Bipolar, S: Stellar

Table A.6: Summary of the colour parameters of our [WR] CSs sample. In the notes column, the abbreviation CB refers to close binary.

serial	PN Name	G	(BP-RP)	E(BP-RP) ^a	(B-V)	E(B-V)	E(BP-RP) ^b	(BP-RP) _o	Note	Ref.
1	PN H 1– 62	14.4	0.77			0.49	0.63	0.14		
2	PN M 2– 20	15.9	1.66			1.29	1.66	0.00		
3	PN H 1– 47	15.7	1.26		0.60	1.21	1.56	– 0.30		
4	PN SwSt 1	11.8	0.85		0.01	0.24	0.31	0.54		
5	PN H 1– 55	16.6	1.13		0.46	0.79	1.02	0.11		
6	PN M 1– 38	14.1	0.93		0.45	0.63	0.81	0.12		
7	PN K 5– 3	19.2	1.1			1.07	1.38	– 0.28		
8	Hen 2– 436	14.9	– 0.06			0.11	0.14	– 0.20		
9	PN M 1– 25	16.6	1.24			0.83	1.07	0.17		
11	PN M 2– 31	17.6	0.66		– 0.30	0.91	1.17	– 0.51		
12	PN M 3– 15	17.5	1.3			1.16	1.50	– 0.20		
13	PN M 2– 34	15.6	1.88			1.00	1.29	0.59		
14	NGC 6629	12.7	0.49		0.33	0.57	0.73	– 0.24		
15	NGC 6578	15.4	0.86		0.48	0.93	1.20	– 0.34		
16	PN SB 17	17.3	2.03	0.0093				2.02		
17	NGC 6567	14.2	0.05		0.06	0.48	0.62	– 0.57		
21	PN M 1– 60	17.4	1.01			1.00	1.29	– 0.28		
23	PN M 2– 43	16.3	1.95			1.58	2.04	– 0.09		
24	PN K 3– 18	16.9	2.1	2.1961				– 0.10		
25	PN A66 58	21.0	– 0.06			0.47	0.61	– 0.67		
27	PN M 4– 13	17.7	1.53			1.61	2.08	– 0.55		
28	PN HuDo 1	17.0	2.54	2.2082				0.33		
29	BD+30 3639	10.3	0.5		– 0.54	0.34	0.44	0.06		
30	Hen 2– 459	15.8	1.82		1.43	1.12	1.44	0.38		
31	PN A66 78	13.1	– 0.3		– 0.19	0.14	0.18	– 0.48		
32	IRAS 21282+5050	13.8	1.76		1.46	1.63	2.10	– 0.34		
33	PN K 3– 61	18.1	1.15		1.10	1.16	1.50	– 0.35		
34	IC 5217	15.6	– 0.34		– 0.10	0.25	0.32	– 0.66		
35	PN Vy 1– 1	14.1	– 0.14		– 0.25	0.26	0.34	– 0.48		
36	NGC 246	11.8	– 0.57		– 0.36	0.02	0.03	– 0.60	CB	1
37	NGC 40	11.5	0.34	0.6188	0.24			– 0.28		
38	PN M 4– 18	13.7	0.78		0.26	0.52	0.67	0.11		
39	IC 2003	16.1	– 0.16		– 0.30	0.21	0.27	– 0.43		
40	PN M 1– 7	19.8	0.17			0.19	0.24	– 0.07		
41	PN A66 30	14.4	– 0.18	0.0001	– 0.06			– 0.18	CB	2
42	PHR J0723+0036	13.8	0.01	0.4190				– 0.41		

Continued on next page

Table A.6 – *Continued from previous page*

serial	PN Name	G	BP-RP	E(BP-RP) ^a	(B-V)	E(B-V)	E(BP-RP) ^b	(BP-RP) _o	Note	Ref.
43	IRAS 06518– 1041	13.9	1.14		0.90	1.16		– 0.02		
44	PN M 1– 11	13.8	1.29		0.81	1.01	1.30	– 0.01		
49	PHR J1134– 5243	13.0	0.21	0.6193				– 0.41	CB	3
55	Hen 2– 99	13.2	0.39	0.7279				– 0.34		
57	PN PM 1– 78	16.2	2.03	1.3390				0.69		
58	RCW 90	17.8	1.89		1.96	2.53		– 0.64		
59	Hen 2– 113	11.6	1.06		0.69	0.86	1.11	– 0.05		
60	Hen 2– 142	14.8	1.24		0.73	1.02	1.31	– 0.07		
61	CPD– 56 8032	11.4	1		0.63	0.65	0.84	0.16		
64	PN H 1– 26	16.8	1.07			1.15	1.48	– 0.41		
65	PN H 2– 1	13.0	0.91		0.40	0.56	0.72	0.19		
66	PN K 2– 16	12.1	0.48	0.8913				– 0.41	CB	3
67	PN H 1– 29	17.0	0.99			1.01	1.30	– 0.31		
69	PN H 1– 9	14.8	1.54		0.80	1.04	1.34	0.20		
71	PN M 1– 27	13.9	1.45	1.2708		0.50	0.81	1.04	0.18	
72	PN H 1– 39	15.5	1.08					0.04		
73	PHR J1752– 3330	14.8	0.95	1.2572				– 0.31	CB	3
74	PN H 1– 43	15.0	1		0.49	0.55	0.71	0.29		
75	PN M 3– 41	15.6	1.44		1.03	1.17	1.51	– 0.07		
76	PN M 3– 17	16.2	1.39		1.00	1.09	1.41	– 0.02		
77	PN M 3– 44	16.0	2.08			1.65	2.13	– 0.05		
79	PN M 2– 27	17.9	1.07			0.99	1.28	– 0.21		
80	PHR J1811– 3042	18.6	0.35	0.0007				0.35		
81	PN Cn 1– 5	15.2	0.36		0.30	0.26	0.34	0.02		
82	NGC 6369	15.5	1.6		1.05	1.31	1.69	– 0.09	CB	3
83	PN Hb 4	17.5	1.1			1.14	1.47	– 0.37		
85	PN M 1– 32	15.7	1.39		1.30	0.94	1.21	0.18		
86	PN M 3– 30	17.8	0.6			0.46	0.59	0.01		
87	PN M 1– 51	18.0	2.15			2.01	2.59	– 0.44		
88	NGC 6751	13.7	– 0.21		0.33	0.43	0.55	– 0.76		
90	PN PC 22	18.0	0.07		0.70	0.44	0.57	– 0.50		
91	NGC 6905	14.6	– 0.19	0.0003				– 0.19	CB	3
92	NGC 7026	15.5	0.64		1.13	0.52	0.67	– 0.03	CB	3
93	IC 1747	15.8	0.36		0.40	0.60	0.77	– 0.41		
94	NGC 1501	14.2	0.6		0.78	0.67	0.86	– 0.26	CB	3
95	PN Ba 1	18.0	0.21		0.30	0.35	0.45	– 0.24		
96	NGC 2371	14.8	– 0.43		– 0.37	0.04	0.05	– 0.48		
98	NGC 2867	15.8	– 0.31		1.70	0.32	0.41	– 0.72	CB	4
99	PN PB 6	17.1	0.1		– 0.20	0.29	0.37	– 0.27		
101	Hen 2– 55	17.0	0.27	0.0004				0.27		
103	BMP J1209– 5553	19.1	0.23			0.39	0.50	– 0.27		
104	PN Th 2– A	16.0	1.79	2.1086				– 0.32	CB	3
105	NGC 5189	14.5	0.04			0.36	0.46	– 0.42	CB	5
106	NGC 5315	13.1	0.38		0.18	0.45	0.58	– 0.20		
107	IRAS 15154– 5258	14.8	2.22	1.2283				0.99		
108	PN PC 14	16.9	– 0.02		0.70	0.41	0.53	– 0.55		
109	MPA J1611– 4356	17.6	0.77	0.0015				0.77		
110	WR 72	13.9	0.26	0.0001	0.04			0.26	CB	3
111	PN SB 34	18.0	0.22	0.0005				0.22		
112	PN M 2– 8	18.6	0.88			0.58	0.75	0.13		
113	PN Hf 2– 1	17.4	0.76			0.50	0.64	0.12		
116	PN M 2– 16	18.4	1.06			0.89	1.15	– 0.09		
117	IC 1297	15.7	– 0.34		0.60	0.10	0.13	– 0.47		
118	PN A66 48	16.8	2.72	2.5016				0.22		
119	PN PB 8	14.3	0.29		0.34	0.28	0.36	– 0.07		
120	IC 4663	16.6	0.05		0.80	0.31	0.40	– 0.35		

(a) Taken from Gaia database, (2) Computed using Eq. 1 (see text in Section 5).

(1) Adam & Mugrauer (2014), (2) Jacoby et al. (2020), (3) Chornay et al. (2021), (4) Aller et al. (2020), (5) Manick et al. (2015).